Charged lepton flavor violation in the $B-L$ symmetric SSM

Xing-Xing Dong,[1,2,3,*] Shu-Min Zhao,[1,2,3,†] Jia-Peng Huo,[1,2,3] Tong-Tong Wang,[1,2,3,‡] and Tai-Fu Feng[1,2,3,4,§]

[1]*College of Physics Science and Technology, Hebei University, Baoding 071002, China*
[2]*Hebei Key Laboratory of High-precision Computation and Application of Quantum Field Theory, Baoding 071002, China*
[3]*Hebei Research Center of the Basic Discipline for Computational Physics, Baoding 071002, China*
[4]*Department of Physics, Chongqing University, Chongqing 401331, China*

(Received 25 June 2023; accepted 23 February 2024; published 13 March 2024)

Charged lepton flavor violation (CLFV) represents a clear new physics (NP) signal beyond the standard model (SM). In this work, we investigate CLFV processes $l_j^- \to l_i^- \gamma$ utilizing mass insertion approximation (MIA) in the minimal supersymmetric extension of the SM with local $B-L$ gauge symmetry ($B-L$ SSM). The MIA method can provide a set of simple analytic formulas for the form factors and the associated effective vertices, so that the movement of the CLFV decays $l_j^- \to l_i^- \gamma$ with the sensitive parameters will be intuitively analyzed. Considering the SM-like Higgs boson mass and the muon anomalous dipole moment (MDM) within 4σ, 3σ, and 2σ regions, we discuss the corresponding constraints on the relevant parameter space of the model.

DOI: 10.1103/PhysRevD.109.055019

I. INTRODUCTION

Although the Standard Model (SM) is considered as a very mature theory, it holds that lepton number is conserved, i.e., no charged lepton flavor violation (CLFV) occurs [1]. However, the CLFV processes can easily occur in new physics (NP) beyond the SM. Therefore, if the CLFV signals are observed in future experiments, it is obvious evidence of NP beyond the SM. In Table I, we show the latest experimental data for the CLFV processes $l_j^- \to l_i^- \gamma$ [2–4], and these processes were discussed in various theoretical frameworks [5–13]. In this work, we investigate these CLFV processes in the minimal supersymmetric extension of the SM with local $B-L$ gauge symmetry ($B-L$ SSM) [14–18]. We hope to reveal some properties of high-energy physics through detailed analyses of these CLFV processes.

It is worth noting that we use a novel calculation method called mass insertion approximation (MIA) [19–24] to study CLFV processes $l_j^- \to l_i^- \gamma$ in the $B-L$ SSM. The CLFV decays $l_j^- \to l_i^- \gamma$ are produced via one-loop contributions, which are influenced by the flavor mixing among the three generations of the $B-L$ SSM sleptons and/or sneutrinos. The MIA works with the sleptons (sneutrinos) in the electroweak interaction eigenstate instead of mass eigenstate. That is to say, the MIA method operates mass insertions inside the propagators of the electroweak interaction sleptons (sneutrinos) eigenstates, instead of performing the exact diagonalization of the mass basis involved in the full one-loop computation. The MIA method has been studied in other LFV works, including the $h, H, A \to \tau\mu$ decays induced from supersymmetric (SUSY) loops [20], an effective LFV $H l_i l_j$ vertex from right-handed neutrinos [21], a one-loop effective LFV $Z l_k l_m$ vertex from heavy neutrinos [22], LFV decays $l_j \to l_i \gamma$ in the $U(1)_X$ SSM [24], and so on. These works provide references and guidance for our research of CLFV processes $l_j^- \to l_i^- \gamma$ in the $B-L$ SSM.

On the base of the minimum supersymmetric Standard Model (MSSM) [25–28], $B-L$ SSM extends the gauge symmetry group to $SU(3)_C \otimes SU(2)_L \otimes U(1)_Y \otimes U(1)_{B-L}$, where B represents the baryon number and L stands for the lepton number. The $B-L$ SSM adds two

TABLE I. The latest experiment limits for the CLFV processes $l_j^- \to l_i^- \gamma$.

CLFV process	Present limit	Confidence level (C.L.)
$\mu \to e\gamma$	$< 4.2 \times 10^{-13}$ [2]	90%
$\tau \to e\gamma$	$< 3.3 \times 10^{-8}$ [3]	90%
$\tau \to \mu\gamma$	$< 4.2 \times 10^{-8}$ [4]	90%

*dongxx@hbu.edu.cn
†zhaosm@hbu.edu.cn
‡wtt961018@163.com
§fengtf@hbu.edu.cn

singlet Higgs superfields $\hat{\eta}$ and $\hat{\bar{\eta}}$ and three generations of right-handed neutrinos superfields $\hat{\nu}_i^c$ to the MSSM. The invariance under $U(1)_{B-L}$ gauge group imposes the R-parity conservation, which is assumed in the MSSM, to avoid proton decay [29]. Besides, through the additional singlet Higgs states and right-handed (s)neutrinos, additional parameter space in the $B-L$ SSM is released from the LEP, Tevatron, and LHC constraints to alleviate the hierarchy problem of the MSSM [30,31]. Furthermore, the $B-L$ SSM can provide much more dark matter (DM) candidates than that in the MSSM [32–35].

Our research of CLFV processes $l_j^- \to l_i^- \gamma$ in the $B-L$ SSM possesses much differences comparing that of $U(1)_X$ SSM. Firstly, because the two models contain different fields, and the corresponding quantum numbers are different, the two works are discussed under different models. In the $U(1)_X$ SSM, three Higgs singlets and right-handed neutrinos are added to MSSM. This model relieves the so-called little hierarchy problem that appears in the MSSM. $\hat{S}$ is the singlet Higgs superfield with a nonzero vacuum expectation value (VEV) $v_s/\sqrt{2}$. The terms $\mu \hat{H}_u \hat{H}_d$ and $\lambda_H \hat{S} \hat{H}_u \hat{H}_d$ can produce an effective $\mu_{\rm eff} = \mu + \lambda_H v_s/\sqrt{2}$, which relieves the μ problem. Comparing this with the condition in MSSM, the lightest CP-even Higgs mass at tree level is improved. The second light neutral CP-even Higgs can be at TeV order. Then it easily satisfies the constraints for heavy Higgs from experiments. Secondly, the two models contain different parameters, so there are big differences in the analytical calculations, analyses at the analytical level, and numerical discussions. In our work, we further discuss the numerical results changing with sensitive parameters within 4σ, 3σ, and 2σ specifically. We study the two-dimensional distribution of sensitive parameters under experimental constraints, and then the influences of some sensitive parameters on ${\rm Br}(l_j^- \to l_i^- \gamma)$ are discussed by one-dimensional graphs. There are some differences in numerical discussion methods and ideas comparing $l_j \to l_i \gamma$ in the $U(1)_X$ SSM with LFV decays.

Depending on the mass eigenstates of the particle and rotation matrices, the mass eigenstate method is often not intuitive and clear enough to find the sensitive parameters, which leads us to pay too much attention to many unimportant parameters. However, the MIA method provides very simple analytic formulas for the form factors involved, which can be written explicitly in terms of the sensitive parameters after a proper expansion. We can easily find the direct impacts of sensitive parameters on CLFV at the analytic level. Therefore, using the MIA method to study CLFV processes provides a new way to study other CLFV processes in the future.

The paper is organized as follows. In Sec. II we introduce the $B-L$ SSM briefly including the superpotential and the general soft breaking terms. In Sec. III we give analytic expressions for muon MDM and the CLFV ratios ${\rm Br}(l_j^- \to l_i^- \gamma)$ in the $B-L$ SSM. The numerical analyses are given in Sec. IV, and the conclusion is discussed in Sec. V. The tedious formulas are collected in Appendix A. In Appendix B we discuss chirality flips with two examples, and demonstrate that the chirality flips occurring in the internal gaugino lines may yield dominant contributions compared to the external lepton lines. In Appendix C we emphasize that the contributions from the incident lepton is dominant by comparing the amplitudes of Figs. 2(a1) and 2(a2).

II. THE $B-L$ SSM

A. The $B-L$ SSM

The $B-L$ SSM extends the superfields of the MSSM by introducing $U(1)_{B-L}$ gauge superfield. Therefore, the local gauge group of the $B-L$ SSM is defined as $SU(3)_C \otimes SU(2)_L \otimes U(1)_Y \otimes U(1)_{B-L}$. Compared with the MSSM, the $B-L$ SSM adds two singlet Higgs superfields, $\hat{\eta}$ and $\hat{\bar{\eta}}$, and three generations of right-handed neutrino superfields $\hat{\nu}_i^c$. In the Table II, we discuss the quantum numbers of gauge symmetry group for the chiral

TABLE II. The chiral superfields and quantum numbers in the $B-L$ SSM.

Superfield	Spin 0	Spin $\frac{1}{2}$	Generations	$U(1)_Y \otimes \mathrm{SU}(2)_L \otimes \mathrm{SU}(3)_C \otimes U(1)_{B-L}$
$\hat{H}_d$	H_d	$\tilde{H}_d$	1	$(-\frac{1}{2}, \mathbf{2}, \mathbf{1}, 0)$
$\hat{H}_u$	H_u	$\tilde{H}_u$	1	$(\frac{1}{2}, \mathbf{2}, \mathbf{1}, 0)$
$\hat{Q}_i$	$\tilde{Q}_i$	Q_i	3	$(\frac{1}{6}, \mathbf{2}, \mathbf{3}, \frac{1}{6})$
$\hat{L}_i$	$\tilde{L}_i$	L_i	3	$(-\frac{1}{2}, \mathbf{2}, \mathbf{1}, -\frac{1}{2})$
$\hat{D}_i^c$	$\tilde{D}_i^c$	D_i^c	3	$(\frac{1}{3}, \mathbf{1}, \bar{\mathbf{3}}, -\frac{1}{6})$
$\hat{U}_i^c$	$\tilde{U}_i^c$	U_i^c	3	$(-\frac{2}{3}, \mathbf{1}, \bar{\mathbf{3}}, -\frac{1}{6})$
$\hat{E}_i^c$	$\tilde{E}_i^c$	E_i^c	3	$(1, \mathbf{1}, \mathbf{1}, \frac{1}{2})$
$\hat{\nu}_i^c$	$\tilde{\nu}_i^c$	ν_i^c	3	$(0, \mathbf{1}, \mathbf{1}, \frac{1}{2})$
$\hat{\eta}$	η	$\tilde{\eta}$	1	$(0, \mathbf{1}, \mathbf{1}, -1)$
$\hat{\bar{\eta}}$	$\bar{\eta}$	$\tilde{\bar{\eta}}$	1	$(0, \mathbf{1}, \mathbf{1}, 1)$

fields in the $B-L$ SSM. Then the $B-L$ SSM superpotential is deduced as

$$W_{B-L} = Y_{u,ij}\hat{Q}_i\hat{H}_u\hat{U}_j^c - Y_{d,ij}\hat{Q}_i\hat{H}_d\hat{D}_j^c + Y_{e,ij}\hat{L}_i\hat{H}_d\hat{E}_j^c + \mu_H\hat{H}_d\hat{H}_u + Y_{x,ij}\hat{\nu}_i^c\hat{\eta}\hat{\nu}_j^c + Y_{\nu,ij}\hat{L}_i\hat{H}_u\hat{\nu}_j^c - \mu_\eta\hat{\eta}\hat{\bar{\eta}}, \quad (1)$$

where i, j represent the generation indices so $Y_{u,ij}$, $Y_{d,ij}$, $Y_{e,ij}$, $Y_{x,ij}$, and $Y_{\nu,ij}$ correspond to the Yukawa coupling coefficients. μ_H and μ_η are both the parameters with mass dimension. μ_H indicates the supersymmetric mass between $SU(2)_L$ Higgs doublets $\hat{H}_d$ and $\hat{H}_u$, and μ_η represents the supersymmetric mass between $U(1)_{B-L}$ Higgs singlets, $\hat{\eta}$ and $\hat{\bar{\eta}}$.

In the $B-L$ SSM, the Higgs doublets and Higgs singlets obtain the nonzero VEVs, then the $SU(2)_L \otimes U(1)_Y \otimes U(1)_{B-L}$ gauge group breaks to $U(1)_{em}$,

$$H_d^0 = \frac{1}{\sqrt{2}}(\phi_d + v_d + i\sigma_d), \qquad H_u^0 = \frac{1}{\sqrt{2}}(\phi_u + v_u + i\sigma_u),$$
$$\eta = \frac{1}{\sqrt{2}}(\phi_\eta + v_\eta + i\sigma_\eta), \qquad \bar{\eta} = \frac{1}{\sqrt{2}}(\phi_{\bar{\eta}} + v_{\bar{\eta}} + i\sigma_{\bar{\eta}}). \quad (2)$$

Here, we define $u^2 = v_\eta^2 + v_{\bar{\eta}}^2$, $v^2 = v_d^2 + v_u^2$ and $\tan\beta' = \frac{v_{\bar{\eta}}}{v_\eta}$ in analogy to the definition $\tan\beta = \frac{v_u}{v_d}$ in the MSSM.

Correspondingly, the soft breaking terms in the $B-L$ SSM are generally written as

$$\mathcal{L}_{\rm soft} = -m_{\tilde{q},ij}^2\tilde{Q}_i^*\tilde{Q}_j - m_{\tilde{u},ij}^2\tilde{U}_i^*\tilde{U}_j - m_{\tilde{d},ij}^2(\tilde{D}_i^c)^*\tilde{D}_j^c - m_{\tilde{L},ij}^2\tilde{L}_i^*\tilde{L}_j - m_{\tilde{E},ij}^2(\tilde{E}_i^c)^*\tilde{E}_j^c$$
$$- m_{H_d}^2|H_d|^2 - m_{H_u}^2|H_u|^2 - m_\eta^2|\eta|^2 - m_{\bar{\eta}}^2|\bar{\eta}|^2 - m_{\tilde{\nu},ij}^2(\tilde{\nu}_i^c)^*\tilde{\nu}_j^c + \Big[-B_\mu H_d H_u$$
$$- B_\eta\eta\bar{\eta} + T_u^{ij}\tilde{Q}_i\tilde{U}_j^c H_u + T_d^{ij}\tilde{Q}_i\tilde{D}_j^c H_d + T_e^{ij}\tilde{L}_i\tilde{E}_j^c H_u + T_\nu^{ij}H_u\tilde{\nu}_i^c\tilde{L}_j + T_x^{ij}\eta\tilde{\nu}_i^c\tilde{\nu}_j^c$$
$$-\frac{1}{2}(M_1\lambda_{\tilde{B}}\lambda_{\tilde{B}} + M_2\lambda_{\tilde{W}}\lambda_{\tilde{W}} + M_3\lambda_{\tilde{g}}\lambda_{\tilde{g}} + 2M_{BB'}\lambda_{\tilde{B}'}\lambda_{\tilde{B}} + M_{B'}\lambda_{\tilde{B}'}\lambda_{\tilde{B}'}) + {\rm H.c.}\Big], \quad (3)$$

where $\lambda_{\tilde{B}}$, $\lambda_{\tilde{W}}$, $\lambda_{\tilde{g}}$ and $\lambda_{\tilde{B}'}$ are the gauginos of $U(1)_Y$, $SU(2)_L$, $SU(3)_C$, and $U(1)_{B-L}$ respectively. Besides, the soft breaking terms of the $B-L$ SSM include the mass squared terms of squarks, sleptons, sneutrinos, and Higgs bosons, the trilinear scalar coupling terms, and the Majorana mass terms.

Compared with the MSSM or other SUSY models, the two Abelian groups in the $B-L$ SSM produce a new effect called as the gauge kinetic mixing. Although both approaches are equivalent, it is easier to work with noncanonical covariant derivatives instead of off-diagonal field-strength tensors in practice. Hence, the covariant derivatives of the $B-L$ SSM can be considered as

$$D_\mu = \partial_\mu - i(Y, B-L)\begin{pmatrix} g_Y, & g'_{YB} \\ g'_{BY}, & g_{B-L}\end{pmatrix}\begin{pmatrix} A_\mu^{\prime Y} \\ A_\mu^{\prime BL}\end{pmatrix}, \quad (4)$$

where Y and $B-L$ correspond to the hypercharge and $B-L$ charge, and $A_\mu^{\prime Y}$ and $A_\mu^{\prime BL}$ denote the gauge fields of $U(1)_Y$ and $U(1)_{B-L}$, respectively. With the condition of the two Abelian gauge groups unbroken, choosing matrix R in a proper form, one can write the coupling matrix as

$$\begin{pmatrix} g_Y, & g'_{YB} \\ g'_{BY}, & g_{B-L}\end{pmatrix}R^T = \begin{pmatrix} g_1, & g_{YB} \\ 0, & g_B\end{pmatrix}, \quad (5)$$

where g_1 corresponds to the measured hypercharge coupling which is modified in $B-L$ SSM as given along with g_B and g_{YB} in Ref. [36]. Then, we can redefine the $U(1)$ gauge fields as

$$R\begin{pmatrix} A_\mu^{\prime Y} \\ A_\mu^{\prime BL}\end{pmatrix} = \begin{pmatrix} A_\mu^{Y} \\ A_\mu^{BL}\end{pmatrix}. \quad (6)$$

The one-loop corrections for the CLFV processes are related with the mass matrices, which can be obtained by SARAH [37,38]. Besides, the CLFV processes in MIA need to consider the trilinear couplings under the interaction eigenstate, so we show some couplings needed in this work as follows. The lepton-charginos CP-even(odd) sneutrinos are deduced as

$$\mathcal{L}_{\bar{l}_j\chi^-\tilde{\nu}^R} = \frac{i}{\sqrt{2}}\bar{l}_j\tilde{\nu}_L^R[Y_l^j P_L\tilde{H}^- + g_2 P_R\tilde{W}^-],$$
$$\mathcal{L}_{\bar{l}_j\chi^-\tilde{\nu}^I} = \frac{1}{\sqrt{2}}\bar{l}_j\tilde{\nu}_L^I[-Y_l^j P_L\tilde{H}^- + g_2 P_R\tilde{W}^-]. \quad (7)$$

The lepton-neutralinos-sleptons are deduced as

$$\mathcal{L}_{\bar{l}_j\chi^0\tilde{L}} = i\bar{l}_j\left\{-\left[\frac{1}{\sqrt{2}}(2g_1P_L\lambda_{\tilde{B}} + (g_B+2g_{YB})P_L\lambda_{\tilde{B}'})\tilde{L}^R + Y_l^jP_L\tilde{H}_d^0\tilde{L}^L\right]\right. \\ \left. + \left[\frac{1}{\sqrt{2}}(g_2P_R\tilde{W}^0 + g_1P_R\lambda_{\tilde{B}} + (g_B+g_{YB})P_R\lambda_{\tilde{B}'})\tilde{L}^L - Y_l^jP_R\tilde{H}_d^0\tilde{L}^R\right]\right\}. \tag{8}$$

B. Higgs mass in the $B-L$ SSM

Due that the strict constraint from SM-like Higgs boson on the numerical results, we discuss the Higgs boson mass matrix. ϕ_d, ϕ_u, ϕ_η, and $\phi_{\bar{\eta}}$ mix together at the tree level. In the basis (ϕ_d, ϕ_u, ϕ_η, $\phi_{\bar{\eta}}$), the tree-level mass squared matrix for neutral CP-even Higgs boson is deduced as

$$M_h^2 = u^2 \times \begin{pmatrix} \frac{1}{4}\frac{g^2x^2}{1+\tan\beta^2} + n^2\tan\beta & -\frac{1}{4}g^2\frac{x^2\tan\beta}{1+\tan\beta^2} - n^2 & \frac{1}{2}g_Bg_{YB}\frac{x}{T} & -\frac{1}{2}g_Bg_{YB}\frac{x\times\tan\beta'}{T} \\ -\frac{1}{4}g^2\frac{x^2\tan\beta}{1+\tan\beta^2} - n^2 & \frac{1}{4}\frac{g^2x^2\tan\beta^2}{1+\tan\beta^2} + \frac{n^2}{\tan\beta} & \frac{1}{2}g_Bg_{YB}\frac{x\times\tan\beta}{T} & \frac{1}{2}g_Bg_{YB}\frac{x\times\tan\beta\times\tan\beta'}{T} \\ \frac{1}{2}g_Bg_{YB}\frac{x}{T} & \frac{1}{2}g_Bg_{YB}\frac{x\times\tan\beta}{T} & \frac{g_B^2}{1+\tan\beta'^2} + \tan\beta'N^2 & -g_B^2\frac{\tan\beta'}{1+\tan\beta'^2} - N^2 \\ -\frac{1}{2}g_Bg_{YB}\frac{x\times\tan\beta'}{T} & \frac{1}{2}g_Bg_{YB}\frac{x\times\tan\beta\times\tan\beta'}{T} & -g_B^2\frac{\tan\beta'}{1+\tan\beta'^2} - N^2 & g_B^2\frac{\tan\beta'^2}{1+\tan\beta'^2} + \frac{N^2}{\tan\beta'} \end{pmatrix}. \tag{9}$$

Here, $g^2 = g_1^2 + g_2^2 + g_{YB}^2$, $T = \sqrt{1+\tan\beta^2}\sqrt{1+\tan\beta'^2}$, $x = \frac{v}{u}$, $n^2 = \frac{\mathrm{Re}(B\mu)}{u^2}$ and $N^2 = \frac{\mathrm{Re}(B_\eta)}{u^2}$. The mass of the SM-like Higgs boson can be obtained after considering the leading-log radiative corrections from stop and top particles [39–41],

$$m_h = \sqrt{(m_{h_1}^0)^2 + \Delta m_h^2}, \tag{10}$$

where $m_{h_1}^0$ represents the lightest tree-level Higgs boson mass, and the leading-log radiative corrections Δm_h^2 can be written as

$$\Delta m_h^2 = \frac{3m_t^4}{4\pi^2v^2}\left[\left(\tilde{t} + \frac{1}{2}\tilde{X}_t\right) + \frac{1}{16\pi^2}\left(\frac{3m_t^2}{2v^2} - 32\pi\alpha_3\right)(\tilde{t}^2 + \tilde{X}_t\tilde{t})\right], \\ \tilde{t} = \log\frac{M_S^2}{m_t^2}, \qquad \tilde{X}_t = \frac{2\tilde{A}_t^2}{M_S^2}\left(1 - \frac{\tilde{A}_t^2}{12M_S^2}\right). \tag{11}$$

Here, α_3 is the strong coupling constant, $M_S = \sqrt{m_{\tilde{t}_1}m_{\tilde{t}_2}}$ with $m_{\tilde{t}_{1,2}}$ are the stop masses, $\tilde{A}_t = A_t - \mu_H\cot\beta$, where $A_t = T_{u,33}$ denotes the trilinear Higgs-stops coupling.

III. THE $(g-2)_\mu$ AND $l_j^- \to l_i^-\gamma$ IN THE $B-L$ SSM

In this section we study the muon MDM and the CLFV processes $l_j^- \to l_i^-\gamma$ in the $B-L$ SSM with the MIA method, which shows the factor of the one-loop contributions more clearly. The concrete contents will be discussed as follows.

A. The one-loop corrections to $(g-2)_\mu$ in the $B-L$ SSM

The effective Lagrangian used here for the muon MDM is given out as follows:

$$\mathcal{L}_{\mathrm{MDM}} = \frac{e}{4m_\mu}a_\mu\bar{l}_\mu\sigma^{\alpha\beta}l_\mu F_{\alpha\beta}, \tag{12}$$

where $\sigma_{\alpha\beta} = i[\gamma_\alpha, \gamma_\beta]/2$, l_μ denotes the wave function of muon, m_μ represents the muon mass, $F_{\alpha\beta}$ is the electromagnetic field strength, and a_μ is the muon MDM.

To obtain the muon MDM, we adopt the effective Lagrangian method [28,42,43], which relates with the following dimension-6 operators:

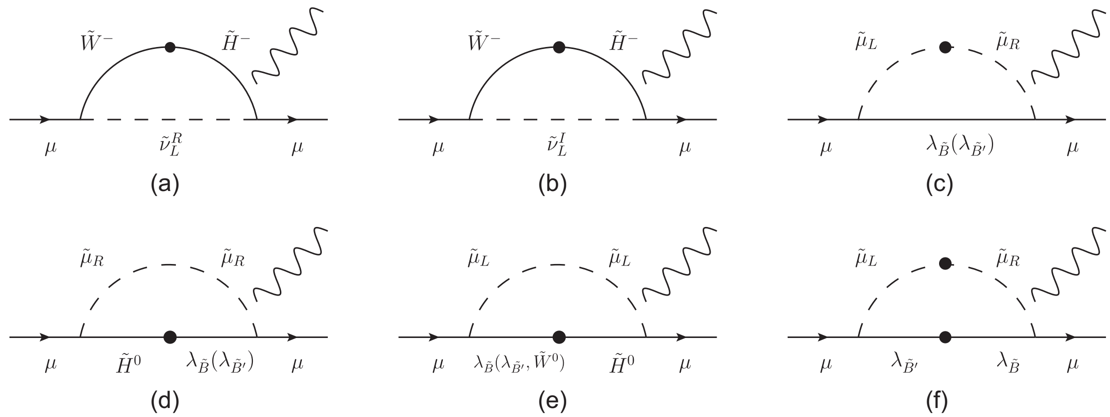

FIG. 1. The Feynman diagrams of muon MDM by MIA in the $B-L$ SSM.

$$\begin{aligned}
&\mathcal{O}_1^{\mp}=\frac{1}{(4\pi)^2}\bar{l}(i\not{\mathcal{D}})^3P_{L,R}l, \qquad \mathcal{O}_2^{\mp}=\frac{eQ_f}{(4\pi)^2}\overline{(i\mathcal{D}_\mu l)}\gamma^\mu F\cdot\sigma P_{L,R}l,\\
&\mathcal{O}_3^{\mp}=\frac{eQ_f}{(4\pi)^2}\bar{l}F\cdot\sigma\gamma^\mu P_{L,R}(i\mathcal{D}_\mu l), \qquad \mathcal{O}_4^{\mp}=\frac{eQ_f}{(4\pi)^2}\bar{l}(\partial^\mu F_{\mu\nu})\gamma^\nu P_{L,R}l,\\
&\mathcal{O}_5^{\mp}=\frac{m_l}{(4\pi)^2}\bar{l}(i\not{\mathcal{D}})^2P_{L,R}l, \qquad \mathcal{O}_6^{\mp}=\frac{eQ_fm_l}{(4\pi)^2}\bar{l}F\cdot\sigma P_{L,R}l,
\end{aligned} \tag{13}$$

with $\mathcal{D}_\mu=\partial_\mu+ieA_\mu$. The operators $\mathcal{O}_{2,3,6}^{\mp}$ have relation with muon MDM when adopting the on shell condition for external leptons. Therefore, we only study the Wilson coefficients $C_{2,3,6}^{\mp}$ of the operators $\mathcal{O}_{2,3,6}^{\mp}$ in the effective Lagrangian. Actually, the Wilson coefficients satisfy the relations $C_2^{\mp}=C_3^{\mp *}$ and $C_6^{+}=C_6^{-*}$. Then the muon MDM can be deduced as

$$a_\mu=\frac{4Q_fm_\mu^2}{(4\pi)^2}\Re(C_2^{+}+C_2^{-*}+C_6^{+}). \tag{14}$$

The Feynman diagrams of muon MDM by MIA in the $B-L$ SSM are shown in Fig. 1. Then, we obtain the concrete forms of the one-loop muon MDM in the $B-L$ SSM adopting the MIA method:

(1) The one-loop contributions from $\tilde{H}^- - \tilde{W}^- - \tilde{\nu}_L^R(\tilde{\nu}_L^I)$,

$$\begin{aligned}
a_\mu(\tilde{\nu}_L^R,\tilde{H}^-,\tilde{W}^-)&=\frac{g_2^2}{2}x_\mu\sqrt{x_2x_{\mu_H}}\tan\beta[2\mathcal{I}(x_{\mu_H},x_{\tilde{\nu}_L^R},x_2)-\mathcal{J}(x_2,x_{\mu_H},x_{\tilde{\nu}_L^R})+2\mathcal{I}(x_2,x_{\tilde{\nu}_L^R},x_{\mu_H})-\mathcal{J}(x_{\mu_H},x_2,x_{\tilde{\nu}_L^R})],\\
a_\mu(\tilde{\nu}_L^I,\tilde{H}^-,\tilde{W}^-)&=\frac{g_2^2}{2}x_\mu\sqrt{x_2x_{\mu_H}}\tan\beta[2\mathcal{I}(x_{\mu_H},x_{\tilde{\nu}_L^I},x_2)-\mathcal{J}(x_2,x_{\mu_H},x_{\tilde{\nu}_L^I})+2\mathcal{I}(x_2,x_{\tilde{\nu}_L^I},x_{\mu_H})-\mathcal{J}(x_{\mu_H},x_2,x_{\tilde{\nu}_L^I})],
\end{aligned} \tag{15}$$

with $x_\mu=\frac{m_\mu^2}{\Lambda^2}$, $x_{\mu_H}=\frac{\mu_H^2}{\Lambda^2}$, and Λ is the NP energy scale. The one-loop functions $\mathcal{I}(x,y,z)$, $\mathcal{J}(x,y,z)$ and the following $f(x,y,z,t)$, $g(x,y,z,t)$, $k(x,y,z,t)$ are collected in the Appendix;

(2) The one-loop contributions from $\lambda_{\tilde{B}}(\lambda_{\tilde{B}'})-\tilde{\mu}_L-\tilde{\mu}_R$,

$$\begin{aligned}
a_\mu(\tilde{\mu}_R,\tilde{\mu}_L,\lambda_{\tilde{B}})&=g_1^2x_\mu\sqrt{x_1x_{\mu_H}}\tan\beta[\mathcal{J}(x_1,x_{\tilde{\mu}_L},x_{\tilde{\mu}_R})+\mathcal{J}(x_1,x_{\tilde{\mu}_R},x_{\tilde{\mu}_L})],\\
a_\mu(\tilde{\mu}_R,\tilde{\mu}_L,\lambda_{\tilde{B}'})&=\frac{(g_B+2g_{YB})(g_B+g_{YB})}{2}x_\mu\sqrt{x_{B'}x_{\mu_H}}\tan\beta[\mathcal{J}(x_{B'},x_{\tilde{\mu}_L},x_{\tilde{\mu}_R})+\mathcal{J}(x_{B'},x_{\tilde{\mu}_R},x_{\tilde{\mu}_L})];
\end{aligned} \tag{16}$$

(3) The one-loop contributions from $\lambda_{\tilde{B}}(\lambda_{\tilde{B}'}) - \tilde{H}^0 - \tilde{\mu}_R$,

$$a_\mu(\tilde{\mu}_R, \lambda_{\tilde{B}}, \tilde{H}^0) = -g_1^2 x_\mu \sqrt{x_1 x_{\mu_H}} \tan\beta[\mathcal{J}(x_1, x_{\mu_H}, x_{\tilde{\mu}_R}) + \mathcal{J}(x_{\mu_H}, x_1, x_{\tilde{\mu}_R})],$$
$$a_\mu(\tilde{\mu}_R, \lambda_{\tilde{B}'}, \tilde{H}^0) = -\frac{(g_B + 2g_{YB})g_{YB}}{2} x_\mu \sqrt{x_{B'} x_{\mu_H}} \tan\beta[\mathcal{J}(x_{B'}, x_{\mu_H}, x_{\tilde{\mu}_R}) + \mathcal{J}(x_{\mu_H}, x_{B'}, x_{\tilde{\mu}_R})]; \tag{17}$$

(4) The one-loop contributions from $\lambda_{\tilde{B}}(\tilde{W}^0, \lambda_{\tilde{B}'}) - \tilde{H}^0 - \tilde{\mu}_L$,

$$a_\mu(\tilde{\mu}_L, \tilde{H}^0, \lambda_{\tilde{B}}) = \frac{1}{2} g_1^2 x_\mu \sqrt{x_1 x_{\mu_H}} \tan\beta[\mathcal{J}(x_1, x_{\mu_H}, x_{\tilde{\mu}_L}) + \mathcal{J}(x_{\mu_H}, x_1, x_{\tilde{\mu}_L})],$$
$$a_\mu(\tilde{\mu}_L, \tilde{H}^0, \tilde{W}^0) = -\frac{1}{2} g_2^2 x_\mu \sqrt{x_2 x_{\mu_H}} \tan\beta[\mathcal{J}(x_2, x_{\mu_H}, x_{\tilde{\mu}_L}) + \mathcal{J}(x_{\mu_H}, x_2, x_{\tilde{\mu}_L})],$$
$$a_\mu(\tilde{\mu}_L, \tilde{H}^0, \lambda_{\tilde{B}'}) = \frac{g_{YB}(g_B + g_{YB})}{2} x_\mu \sqrt{x_{B'} x_{\mu_H}} \tan\beta[\mathcal{J}(x_{B'}, x_{\mu_H}, x_{\tilde{\mu}_L}) + \mathcal{J}(x_{\mu_H}, x_{B'}, x_{\tilde{\mu}_L})]; \tag{18}$$

(5) The one-loop contributions from $\lambda_{\tilde{B}} - \lambda_{\tilde{B}'} - \tilde{\mu}_R - \tilde{\mu}_L$,

$$a_\mu(\tilde{\mu}_R, \tilde{\mu}_L, \lambda_{\tilde{B}}, \lambda_{\tilde{B}'}) = g_1(4g_{YB} + 3g_B) x_\mu \sqrt{x_{BB'} x_{\mu_H}} \tan\beta[\sqrt{x_1 x_{B'}} f(x_{B'}, x_1, x_{\tilde{\mu}_L}, x_{\tilde{\mu}_R}) - g(x_{B'}, x_1, x_{\tilde{\mu}_L}, x_{\tilde{\mu}_R})]. \tag{19}$$

In Eqs. (15)–(19), one can easily find the factors x_μ and $\tan\beta$, which possess the same characteristic as these in MSSM [19]. In the $B-L$ SSM, the new gaugino $\lambda_{\tilde{B}'}$ generates the new contributions to muon MDM, which are deduced in Eqs. (16)–(19).

To obtain clearer images of the results, we suppose that all the superparticle masses are almost degenerate. The author [19] gives the one-loop results of the MSSM in the extreme case where the masses for superparticles M_1, M_2, μ_H, $m_{\tilde{\mu}_L}$, $m_{\tilde{\mu}_R}$ are equal to Λ,

$$a_\mu^{\mathrm{MSSM}} \simeq \frac{1}{192\pi^2} \frac{m_\mu^2}{\Lambda^2} \tan\beta(5g_2^2 + g_1^2). \tag{20}$$

Here, we also use the similar case

$$M_1 = M_2 = \mu_H = m_{\tilde{\nu}_L^R} = m_{\tilde{\nu}_L^I} = m_{\tilde{\mu}_L} = m_{\tilde{\mu}_R} = |M_{B'}| = |M_{BB'}| = \Lambda. \tag{21}$$

Then, the functions $\mathcal{I}(x,y,z)$, $\mathcal{J}(x,y,z)$, $f(x,y,z,t)$, and $g(x,y,z,t)$ can be simplified as

$$\mathcal{I}(1,1,1) = \frac{1}{96\pi^2}, \qquad \mathcal{J}(1,1,1) = \frac{1}{192\pi^2},$$
$$f(1,1,1,1) = -\frac{1}{240\pi^2}, \qquad g(1,1,1,1) = -\frac{1}{960\pi^2}. \tag{22}$$

In this condition, we obtain the simplified one-loop contributions of muon MDM in the $B-L$ SSM.

$$a_\mu^{B-L} \simeq \frac{1}{960\pi^2} \frac{m_\mu^2}{\Lambda^2} \tan\beta[5(5g_2^2 + g_1^2) + 5(g_B^2 + 3g_{YB}g_B + g_{YB}^2)\mathrm{sign}[M_{B'}] + g_1(3g_B + 4g_{YB})\mathrm{sign}[M_{BB'}](1 - 4\mathrm{sign}[M_{B'}])]. \tag{23}$$

In addition to the one-loop MSSM contributions, the Eq. (23) adds considerable corrections to a_μ from the new gaugino $\lambda_{\tilde{B}'}$. In the condition $-0.7 < g_{YB} < -0.05$, $0.1 < g_B < 0.85$ and $|g_{YB}| < g_B < \frac{4}{3}|g_{YB}|$ and with the supposition $\mathrm{sign}[M_{B'}] = \mathrm{sign}[M_{BB'}] = -1$, the corrections beyond MSSM can reach large values,

$$a_\mu^{B-L} \to \frac{1}{192\pi^2} \frac{m_\mu^2}{\Lambda^2} \tan\beta[(5g_2^2 + g_1^2) - (g_1(3g_B + 4g_{YB}) + (g_B^2 + 3g_{YB}g_B + g_{YB}^2))]. \tag{24}$$

Here, the order analysis shows,

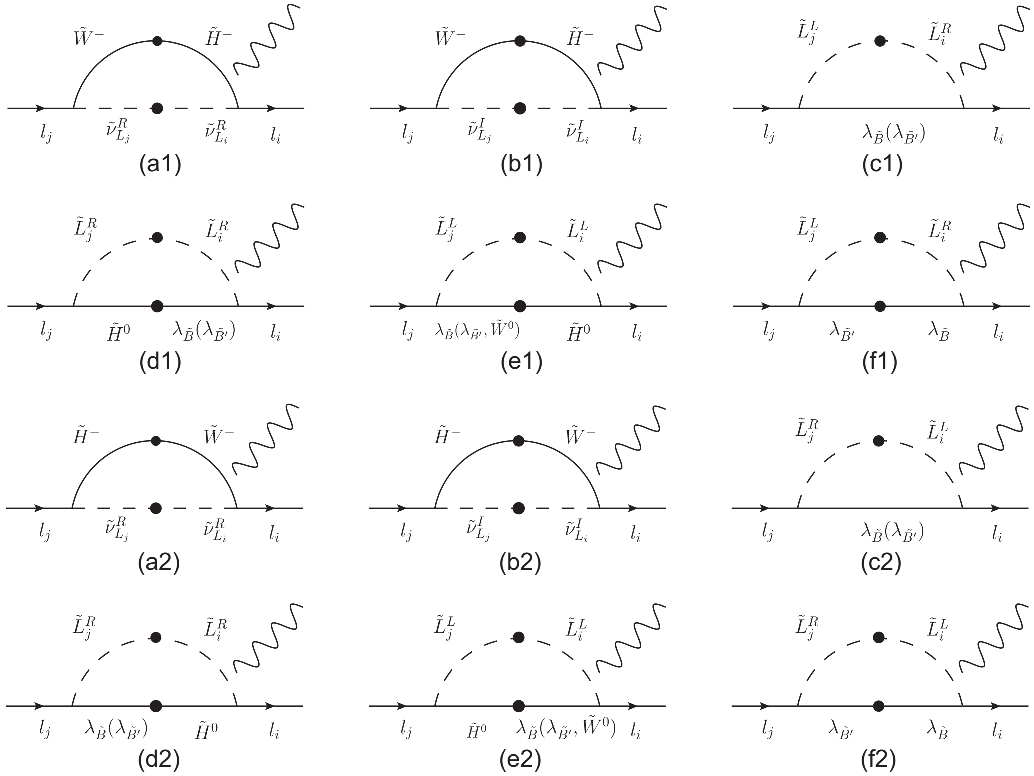

FIG. 2. The Feynman diagrams of $l_j^- \to l_i^- \gamma$ by MIA in the $B-L$ SSM.

$$0 < \frac{-g_1(3g_B + 4g_{YB}) - (g_B^2 + 3g_{YB}g_B + g_{YB}^2)}{5g_2^2 + g_1^2} \lesssim 1. \qquad (25)$$

Therefore, the $B-L$ SSM contributions beyond MSSM are considerable.

B. The one-loop corrections to $l_j^- \to l_i^- \gamma$ in the $B-L$ SSM

Generally, the effective amplitude of the CLFV processes $l_j^- \to l_i^- \gamma$ can be written as

$$\begin{aligned}\mathcal{M} = e\epsilon^\mu \bar{u}_i(p+q)[q^2\gamma_\mu(C_1^L P_L + C_1^R P_R) \\ + m_{l_j} i\sigma_{\mu\nu} q^\nu (C_2^L P_L + C_2^R P_R)]u_j(p),\end{aligned} \qquad (26)$$

where p (q) represents the incident lepton (photon) momentum, m_{l_j} is the jth generation lepton mass, ϵ is the photon polarization vector, and $u_j(p)$ ($\bar{u}_i(p+q)$) is the incident (outgoing) lepton wave function. In Fig. 2, we show the relevant $B-L$ SSM Feynman diagrams of $l_j^- \to l_i^- \gamma$ by MIA. Here, we omit the chirality flips of external lepton in our calculation. In Appendix B we discuss chirality flips with two examples, and demonstrate that the chirality flips occurring in the internal gaugino lines may yield dominant contributions comparing in the external lepton lines. In Appendix C we emphasize the contributions from the incident lepton is dominant by comparing the amplitudes of Figs. 2(a1) and 2(a2). The Wilson coefficients C_α^{iL}, C_α^{iR} ($\alpha = 1, 2, i = 1, \ldots, 5$) adopting the MIA method are obtained from the sum of these diagrams' amplitudes:

(1) The one-loop contributions from $\tilde{H}^- - \tilde{W}^- - \tilde{\nu}_L^R(\tilde{\nu}_L^I)$,

$$\begin{aligned}
C_2^{1L}(\tilde{\nu}_{L_j}^R, \tilde{\nu}_{L_i}^R, \tilde{H}^-, \tilde{W}^-) &= \frac{g_2^2}{2\Lambda^4}\frac{m_{l_i}}{m_{l_j}}\sqrt{x_2 x_{\mu_H}}\Delta_{ij}^{LL}\tan\beta\Big[k(x_{\mu_H}, x_2, x_{\tilde{\nu}_{L_j}^R}, x_{\tilde{\nu}_{L_i}^R}) \\
&\quad + k(x_2, x_{\mu_H}, x_{\tilde{\nu}_{L_j}^R}, x_{\tilde{\nu}_{L_i}^R}) - f(x_2, x_{\mu_H}, x_{\tilde{\nu}_{L_j}^R}, x_{\tilde{\nu}_{L_i}^R})\Big], \\
C_2^{1L}(\tilde{\nu}_{L_j}^I, \tilde{\nu}_{L_i}^I, \tilde{H}^-, \tilde{W}^-) &= \frac{g_2^2}{2\Lambda^4}\frac{m_{l_i}}{m_{l_j}}\sqrt{x_2 x_{\mu_H}}\Delta_{ij}^{LL}\tan\beta\Big[k(x_{\mu_H}, x_2, x_{\tilde{\nu}_{L_j}^I}, x_{\tilde{\nu}_{L_i}^I}) \\
&\quad + k(x_2, x_{\mu_H}, x_{\tilde{\nu}_{L_j}^I}, x_{\tilde{\nu}_{L_i}^I}) - f(x_2, x_{\mu_H}, x_{\tilde{\nu}_{L_j}^I}, x_{\tilde{\nu}_{L_i}^I})\Big],
\end{aligned} \qquad (27)$$

$$C_2^{1R}(\tilde{\nu}^R_{L_j},\tilde{\nu}^R_{L_i},\tilde{H}^-,\tilde{W}^-)=\frac{g_2^2}{2\Lambda^4}\sqrt{x_2x_{\mu_H}}\Delta^{LL}_{ij}\tan\beta\Big[k(x_{\mu_H},x_2,x_{\tilde{\nu}^R_{L_j}},x_{\tilde{\nu}^R_{L_i}})+k(x_2,x_{\mu_H},x_{\tilde{\nu}^R_{L_j}},x_{\tilde{\nu}^R_{L_i}})-f(x_2,x_{\mu_H},x_{\tilde{\nu}^R_{L_j}},x_{\tilde{\nu}^R_{L_i}})\Big],$$
$$C_2^{1R}(\tilde{\nu}^I_{L_j},\tilde{\nu}^I_{L_i},\tilde{H}^-,\tilde{W}^-)=\frac{g_2^2}{2\Lambda^4}\sqrt{x_2x_{\mu_H}}\Delta^{LL}_{ij}\tan\beta\Big[k(x_{\mu_H},x_2,x_{\tilde{\nu}^I_{L_j}},x_{\tilde{\nu}^I_{L_i}})+k(x_2,x_{\mu_H},x_{\tilde{\nu}^I_{L_j}},x_{\tilde{\nu}^I_{L_i}})-f(x_2,x_{\mu_H},x_{\tilde{\nu}^I_{L_j}},x_{\tilde{\nu}^I_{L_i}})\Big];\tag{28}$$

(2) The one-loop contributions from $\lambda_{\tilde{B}}(\lambda_{\tilde{B}'})-\tilde{L}^L_j-\tilde{L}^R_i$,

$$C_2^{2L}(\tilde{L}^L_j,\tilde{L}^R_i,\lambda_{\tilde{B}})=-\frac{g_1^2}{2\Lambda^3m_{l_j}}\sqrt{x_1}\Delta^{LR}_{ij}\Big[\mathcal{J}(x_1,x_{\tilde{L}^L_j},x_{\tilde{L}^R_i})+\mathcal{J}(x_1,x_{\tilde{L}^R_i},x_{\tilde{L}^L_j})\Big],$$
$$C_2^{2L}(\tilde{L}^L_j,\tilde{L}^R_i,\lambda_{\tilde{B}'})=-\frac{(g_B+2g_{YB})(g_B+g_{YB})}{4\Lambda^3m_{l_j}}\sqrt{x_{B'}}\Delta^{LR}_{ij}\Big[\mathcal{J}(x_{B'},x_{\tilde{L}^L_j},x_{\tilde{L}^R_i})+\mathcal{J}(x_{B'},x_{\tilde{L}^R_i},x_{\tilde{L}^L_j})\Big],\tag{29}$$

$$C_2^{2R}(\tilde{L}^R_j,\tilde{L}^L_i,\lambda_{\tilde{B}})=-\frac{g_1^2}{2\Lambda^3m_{l_j}}\sqrt{x_1}\Delta^{LR}_{ij}\Big[\mathcal{J}(x_1,x_{\tilde{L}^R_j},x_{\tilde{L}^L_i})+\mathcal{J}(x_1,x_{\tilde{L}^L_i},x_{\tilde{L}^R_j})\Big],$$
$$C_2^{2R}(\tilde{L}^R_j,\tilde{L}^L_i,\lambda_{\tilde{B}'})=-\frac{(g_B+2g_{YB})(g_B+g_{YB})}{4\Lambda^3m_{l_j}}\sqrt{x_{B'}}\Delta^{LR}_{ij}\Big[\mathcal{J}(x_{B'},x_{\tilde{L}^R_j},x_{\tilde{L}^L_i})+\mathcal{J}(x_{B'},x_{\tilde{L}^L_i},x_{\tilde{L}^R_j})\Big];\tag{30}$$

(3) The one-loop contributions from $\lambda_{\tilde{B}}(\lambda_{\tilde{B}'})-\tilde{H}^0-\tilde{L}^R_j-\tilde{L}^R_i$:

$$C_2^{3L}(\tilde{L}^R_j,\tilde{L}^R_i,\lambda_{\tilde{B}},\tilde{H}^0)=-\frac{g_1^2}{\Lambda^4}\Delta^{RR}_{ij}\Big[\sqrt{x_1x_{\mu_H}}\tan\beta f(x_1,x_{\mu_H},x_{\tilde{L}^R_j},x_{\tilde{L}^R_i})-g(x_1,x_{\mu_H},x_{\tilde{L}^R_j},x_{\tilde{L}^R_i})\Big],$$
$$C_2^{3L}(\tilde{L}^R_j,\tilde{L}^R_i,\lambda_{\tilde{B}'},\tilde{H}^0)=-\frac{(g_B+2g_{YB})g_{YB}}{2\Lambda^4}\Delta^{RR}_{ij}\Big[\sqrt{x_{B'}x_{\mu_H}}\tan\beta f(x_{B'},x_{\mu_H},x_{\tilde{L}^R_j},x_{\tilde{L}^R_i})-g(x_{B'},x_{\mu_H},x_{\tilde{L}^R_j},x_{\tilde{L}^R_i})\Big],\tag{31}$$

$$C_2^{3R}(\tilde{L}^R_j,\tilde{L}^R_i,\lambda_{\tilde{B}},\tilde{H}^0)=-\frac{g_1^2}{\Lambda^4}\frac{m_{l_i}}{m_{l_j}}\Delta^{RR}_{ij}\Big[\sqrt{x_1x_{\mu_H}}\tan\beta f(x_1,x_{\mu_H},x_{\tilde{L}^R_j},x_{\tilde{L}^R_i})-g(x_1,x_{\mu_H},x_{\tilde{L}^R_j},x_{\tilde{L}^R_i})\Big],$$
$$C_2^{3R}(\tilde{L}^R_j,\tilde{L}^R_i,\lambda_{\tilde{B}'},\tilde{H}^0)=-\frac{(g_B+2g_{YB})g_{YB}}{2\Lambda^4}\frac{m_{l_i}}{m_{l_j}}\Delta^{RR}_{ij}\Big[\sqrt{x_{B'}x_{\mu_H}}\tan\beta f(x_{B'},x_{\mu_H},x_{\tilde{L}^R_j},x_{\tilde{L}^R_i})-g(x_{B'},x_{\mu_H},x_{\tilde{L}^R_j},x_{\tilde{L}^R_i})\Big];\tag{32}$$

(4) The one-loop contributions from $\lambda_{\tilde{B}}(\tilde{W}^0,\lambda_{\tilde{B}'})-\tilde{H}^0-\tilde{L}^L_j-\tilde{L}^L_i$:

$$C_2^{4L}(\tilde{L}^L_j,\tilde{L}^L_i,\tilde{H}^0,\lambda_{\tilde{B}})=\frac{g_1^2}{2\Lambda^4}\frac{m_{l_i}}{m_{l_j}}\Delta^{LL}_{ij}\Big[\sqrt{x_1x_{\mu_H}}\tan\beta f(x_1,x_{\mu_H},x_{\tilde{L}^L_j},x_{\tilde{L}^L_i})-g(x_1,x_{\mu_H},x_{\tilde{L}^L_j},x_{\tilde{L}^L_i})\Big],$$
$$C_2^{4L}(\tilde{L}^L_j,\tilde{L}^L_i,\tilde{H}^0,\tilde{W}^0)=-\frac{g_2^2}{2\Lambda^4}\frac{m_{l_i}}{m_{l_j}}\Delta^{LL}_{ij}\Big[\sqrt{x_2x_{\mu_H}}\tan\beta f(x_2,x_{\mu_H},x_{\tilde{L}^L_j},x_{\tilde{L}^L_i})-g(x_2,x_{\mu_H},x_{\tilde{L}^L_j},x_{\tilde{L}^L_i})\Big],$$
$$C_2^{4L}(\tilde{L}^L_j,\tilde{L}^L_i,\tilde{H}^0,\lambda_{\tilde{B}'})=\frac{g_{YB}(g_B+g_{YB})}{2\Lambda^4}\frac{m_{l_i}}{m_{l_j}}\Delta^{LL}_{ij}\Big[\sqrt{x_{B'}x_{\mu_H}}\tan\beta f(x_{B'},x_{\mu_H},x_{\tilde{L}^L_j},x_{\tilde{L}^L_i})-g(x_{B'},x_{\mu_H},x_{\tilde{L}^L_j},x_{\tilde{L}^L_i})\Big],\tag{33}$$

$$C_2^{4R}(\tilde{L}^L_j,\tilde{L}^L_i,\tilde{H}^0,\lambda_{\tilde{B}})=\frac{g_1^2}{2\Lambda^4}\Delta^{LL}_{ij}\Big[\sqrt{x_1x_{\mu_H}}\tan\beta f(x_1,x_{\mu_H},x_{\tilde{L}^L_j},x_{\tilde{L}^L_i})-g(x_1,x_{\mu_H},x_{\tilde{L}^L_j},x_{\tilde{L}^L_i})\Big],$$
$$C_2^{4R}(\tilde{L}^L_j,\tilde{L}^L_i,\tilde{H}^0,\tilde{W}^0)=-\frac{g_2^2}{2\Lambda^4}\Delta^{LL}_{ij}\Big[\sqrt{x_2x_{\mu_H}}\tan\beta f(x_2,x_{\mu_H},x_{\tilde{L}^L_j},x_{\tilde{L}^L_i})-g(x_2,x_{\mu_H},x_{\tilde{L}^L_j},x_{\tilde{L}^L_i})\Big],$$
$$C_2^{4R}(\tilde{L}^L_j,\tilde{L}^L_i,\tilde{H}^0,\lambda_{\tilde{B}'})=\frac{g_{YB}(g_B+g_{YB})}{2\Lambda^4}\Delta^{LL}_{ij}\Big[\sqrt{x_{B'}x_{\mu_H}}\tan\beta f(x_{B'},x_{\mu_H},x_{\tilde{L}^L_j},x_{\tilde{L}^L_i})-g(x_{B'},x_{\mu_H},x_{\tilde{L}^L_j},x_{\tilde{L}^L_i})\Big].\tag{34}$$

(5) The one-loop contributions from $\lambda_{\tilde{B}} - \lambda_{\tilde{B}'} - \tilde{L}_j^L - \tilde{L}_i^R$:

$$C_2^{5L}(\tilde{L}_j^L, \tilde{L}_i^R, \lambda_{\tilde{B}}, \lambda_{\tilde{B}'}) = -\frac{g_1(4g_{YB}+3g_B)}{2\Lambda^3 m_{l_j}}\sqrt{x_{BB'}}\Delta_{ij}^{LR}\left[\sqrt{x_1 x_{B'}} f(x_{B'}, x_1, x_{\tilde{L}_j^L}, x_{\tilde{L}_i^R}) - g(x_{B'}, x_1, x_{\tilde{L}_j^L}, x_{\tilde{L}_i^R})\right], \tag{35}$$

$$C_2^{5R}(\tilde{L}_j^R, \tilde{L}_i^L, \lambda_{\tilde{B}}, \lambda_{\tilde{B}'}) = -\frac{g_1(4g_{YB}+3g_B)}{2\Lambda^3 m_{l_j}}\sqrt{x_{BB'}}\Delta_{ij}^{LR}\left[\sqrt{x_1 x_{B'}} f(x_{B'}, x_1, x_{\tilde{L}_j^R}, x_{\tilde{L}_i^L}) - g(x_{B'}, x_1, x_{\tilde{L}_j^R}, x_{\tilde{L}_i^L})\right]. \tag{36}$$

Then the decay width of $l_j^- \to l_i^- \gamma$ can be written as

$$\Gamma(l_j^- \to l_i^- \gamma) = \frac{e^2}{16\pi} m_{l_j}^5 (|C_2^L|^2 + |C_2^R|^2), \tag{37}$$

with the final Wilson coefficient $C_2^{L,R} = \sum_i^{i=1\ldots5} C_2^{iL,iR}$, $i = 1, \ldots, 5$. And the branching ratio for $l_j^- \to l_i^- \gamma$ is

$$\mathrm{Br}(l_j^- \to l_i^- \gamma) = \Gamma(l_j^- \to l_i^- \gamma)/\Gamma_{l_j}. \tag{38}$$

From Eqs. (27)–(36), we find that $C_2^{L,R}$ are almost affected by $\tan\beta$ and $\Delta_{ij}^{AB}(A, B = L, R)$. Here, $\Delta_{ij}^{LL} = m_L^2 \delta_{ij}^{LL}$, $\Delta_{ij}^{RR} = m_E^2 \delta_{ij}^{RR}$, and $\Delta_{ij}^{LR} = A_e v_d \delta_{ij}^{LR}$, which are related with soft breaking slepton mass-squared matrices $m^2_{\tilde{L},\tilde{E}}$ and the trilinear coupling matrix T_e, whose off-diagonal terms introduce the slepton flavor mixing,

$$m_{\tilde{L}}^2 = \begin{pmatrix} 1, & \delta_{12}^{LL}, & \delta_{13}^{LL} \\ \delta_{12}^{LL}, & 1, & \delta_{23}^{LL} \\ \delta_{13}^{LL}, & \delta_{23}^{LL}, & 1 \end{pmatrix} m_L^2, \qquad m_{\tilde{E}}^2 = \begin{pmatrix} 1, & \delta_{12}^{RR}, & \delta_{13}^{RR} \\ \delta_{12}^{RR}, & 1, & \delta_{23}^{RR} \\ \delta_{13}^{RR}, & \delta_{23}^{RR}, & 1 \end{pmatrix} m_E^2, \qquad T_e = \begin{pmatrix} 1, & \delta_{12}^{LR}, & \delta_{13}^{LR} \\ \delta_{12}^{LR}, & 1, & \delta_{23}^{LR} \\ \delta_{13}^{LR}, & \delta_{23}^{LR}, & 1 \end{pmatrix} A_e. \tag{39}$$

In the subsequent numerical analyses, we discuss the branching ratios for CLFV processes $l_j^- \to l_i^- \gamma$ in the $B-L$ SSM depending on the slepton mixing parameters.

In order to more intuitively analyze the factors that affect CLFV processes $l_j^- \to l_i^- \gamma$, we also suppose that the superparticles masses are almost degenerate. In other words, we give the one-loop results in the extreme case where the super particle masses are equal to Λ,

$$|M_1| = |M_2| = |\mu_H| = m_L = m_E = |M_{B'}| = |M_{BB'}| = \Lambda. \tag{40}$$

Here, the function $k(x, y, z, t)$ is much simplified as $k(1, 1, 1, 1) = -\frac{1}{192\pi^2}$, then the Wilson coefficients from the MSSM can be deduced as

$$C_2^{\mathrm{L,MSSM}} \simeq \frac{1}{1920\pi^2\Lambda^4 m_{l_j}}\left[-10\sqrt{2}g_1^2 \Lambda A_e v_d \mathrm{sign}[M_1]\delta_{ij}^{LR} + 2g_1^2(4\tan\beta\,\mathrm{sign}[M_1\mu_H] - 1)m_{l_j} m_E^2 \delta_{ij}^{RR}\right], \tag{41}$$

$$\begin{aligned} C_2^{\mathrm{R,MSSM}} \simeq \frac{1}{1920\pi^2\Lambda^4 m_{l_j}}\Big[&-10\sqrt{2}g_1^2 \Lambda A_e v_d \mathrm{sign}[M_1]\delta_{ij}^{LR} - (g_2^2(8\tan\beta\,\mathrm{sign}[M_2\mu_H] + 1) \\ &+ g_1^2(4\tan\beta\,\mathrm{sign}\Big[M_1\mu_H\Big] - 1))m_{l_j} m_L^2 \delta_{ij}^{LL}\Big]. \end{aligned} \tag{42}$$

With the supposition $\mathrm{sign}[M_1] = \mathrm{sign}[\mu_H] = \mathrm{sign}[M_2] = 1$ and $4\tan\beta \gg 1$, the one-loop corrections to the Wilson coefficient of MSSM can reach

$$C_2^{\mathrm{L,MSSM}} \to \frac{1}{1920\pi^2\Lambda^2 m_{l_j}}\left[-10\sqrt{2}g_1^2 \frac{A_e v_d}{\Lambda}\delta_{ij}^{LR} + 8g_1^2 \tan\beta\, m_{l_j} \delta_{ij}^{RR}\right], \tag{43}$$

$$C_2^{\mathrm{R,MSSM}} \to \frac{1}{1920\pi^2\Lambda^2 m_{l_j}}\left[-10\sqrt{2}g_1^2\frac{A_e v_d}{\Lambda}\delta_{ij}^{LR} - (8g_2^2+4g_1^2)\tan\beta m_{l_j}\delta_{ij}^{LL}\right]. \tag{44}$$

In the same way, the Wilson coefficient from the B-LSSM can be written as

$$\begin{aligned} C_2^{\mathrm{L,B-L}} \simeq -\frac{1}{3840\pi^2\Lambda^4 m_{l_j}}\Big[&\sqrt{2}(20g_1^2\mathrm{sign}[M_1]+10(g_B+g_{YB})(g_B+2g_{YB})\mathrm{sign}[M_{B'}] \\ &- g_1(3g_B+4g_{YB})\mathrm{sign}[M_{BB'}](4\mathrm{sign}[M_1M_{B'}]-1))\Lambda A_e v_d\delta_{ij}^{LR} - 2(g_1^2(8\tan\beta\mathrm{sign}[\mu_H M_1]-2) \\ &+ g_{YB}(g_B+2g_{YB})(4\tan\beta\mathrm{sign}[\mu_H M_{B'}]-1))m_{l_j}m_E^2\delta_{ij}^{RR}\Big], \end{aligned} \tag{45}$$

$$\begin{aligned} C_2^{\mathrm{R,B-L}} \simeq -\frac{1}{3840\pi^2\Lambda^4 m_{l_j}}\Big[&\sqrt{2}(20g_1^2\mathrm{sign}[M_1]+10(g_B+g_{YB})(g_B+2g_{YB})\mathrm{sign}[M_{B'}] \\ &- g_1(3g_B+4g_{YB})\mathrm{sign}[M_{BB'}](4\mathrm{sign}[M_1M_{B'}]-1))\Lambda A_e v_d\delta_{ij}^{LR} \\ &+ 2(g_2^2(8\tan\beta\mathrm{sign}[\mu_H M_2]+1)+g_1^2(4\tan\beta\mathrm{sign}[\mu_H M_1]-1) \\ &+ g_{YB}(g_B+g_{YB})(4\tan\beta\mathrm{sign}[\mu_H M_{B'}]-1))m_{l_j}m_L^2\delta_{ij}^{LL}\Big]. \end{aligned} \tag{46}$$

With the supposition $\mathrm{sign}[M_1]=\mathrm{sign}[M_2]=\mathrm{sign}[\mu_H]=1$, $\mathrm{sign}[M_{B'}]=\mathrm{sign}[M_{BB'}]=-1$ and $4\tan\beta\gg 1$, the Wilson coefficient for the $B-L$ SSM can be

$$\begin{aligned} C_2^{\mathrm{L,B-L}} \to \frac{1}{3840\pi^2\Lambda^2 m_{l_j}}\Big[&-20\sqrt{2}g_1^2\frac{A_e v_d}{\Lambda}\delta_{ij}^{LR}+16g_1^2\tan\beta m_{l_j}\delta_{ij}^{RR}+\sqrt{2}(10(g_B+g_{YB})(g_B+2g_{YB}) \\ &+5g_1(3g_B+4g_{YB}))\frac{A_e v_d}{\Lambda}\delta_{ij}^{LR}-8g_{YB}(g_B+2g_{YB})\tan\beta m_{l_j}\delta_{ij}^{RR}\Big], \end{aligned} \tag{47}$$

$$\begin{aligned} C_2^{\mathrm{R,B-L}} \to \frac{1}{3840\pi^2\Lambda^2 m_{l_j}}\Big[&-20\sqrt{2}g_1^2\frac{A_e v_d}{\Lambda}\delta_{ij}^{LR}-2(8g_2^2+4g_1^2)\tan\beta m_{l_j}\delta_{ij}^{LL}+\sqrt{2}(10(g_B+g_{YB})(g_B+2g_{YB}) \\ &+5g_1(3g_B+4g_{YB}))\frac{A_e v_d}{\Lambda}\delta_{ij}^{LR}+8g_{YB}(g_B+g_{YB})\tan\beta m_{l_j}\delta_{ij}^{LL}\Big]. \end{aligned} \tag{48}$$

In the condition $-0.7<g_{YB}<-0.05$, $0.1<g_B<0.85$, and $|g_{YB}|<g_B<4/3|g_{YB}|$, then $\sqrt{2}(10(g_B+g_{YB})(g_B+2g_{YB})+5g_1(3g_B+4g_{YB}))<0$, $-8g_{YB}(g_B+2g_{YB})<0$, $8g_{YB}(g_B+g_{YB})<0$. The order analysis shows

$$D_2^{L,B-L}=\left[\sqrt{2}(10(g_B+g_{YB})(g_B+2g_{YB})+5g_1(3g_B+4g_{YB}))\frac{A_e v_d}{\Lambda}\delta_{ij}^{LR}-8g_{YB}(g_B+2g_{YB})\tan\beta m_{l_j}\delta_{ij}^{RR}\right]<0, \tag{49}$$

$$D_2^{R,B-L}=\left[\sqrt{2}(10(g_B+g_{YB})(g_B+2g_{YB})+5g_1(3g_B+4g_{YB}))\frac{A_e v_d}{\Lambda}\delta_{ij}^{LR}+8g_{YB}(g_B+g_{YB})\tan\beta m_{l_j}\delta_{ij}^{LL}\right]<0. \tag{50}$$

As parameters $g_1\simeq 0.3$, $g_2\simeq 0.6$, $g_B\simeq 0.3$, $g_{YB}\simeq -0.25$, $\tan\beta m_\mu\simeq\frac{A_e v_d}{\Lambda}\simeq 1$, $\delta_{12}^{LL}\simeq\delta_{12}^{RR}\simeq\delta_{12}^{LR}\simeq 10^{-5}$, $D_2^{L,B-L}$, and $D_2^{R,B-L}$ are at the order around -10^{-5}, which approximately take the same values as the MSSM contributions from $[-10\sqrt{2}g_1^2\frac{A_e v_d}{\Lambda}\delta_{ij}^{LR}+8g_1^2\tan\beta m_{l_j}\delta_{ij}^{RR}]$ and $[-10\sqrt{2}g_1^2\frac{A_e v_d}{\Lambda}\delta_{ij}^{LR}-(8g_2^2+4g_1^2)\tan\beta m_{l_j}\delta_{ij}^{LL}]$. Therefore, the $B-L$ SSM contributions beyond MSSM are considerable.

IV. THE NUMERICAL RESULTS

In this section, we research the numerical results of the branching ratios for CLFV processes $l_j^-\to l_i^-\gamma$. We consider some experimental constraints: (1) The updated experimental data indicates that the Z' boson mass satisfies $M_Z'\geq 5.15$ TeV with 95% C.L. [44]. Refs. [45,46] give us an upper bound on the ratio between the mass of Z' boson and its gauge coupling at 99% C.L.: $\frac{M_Z'}{g_B}\geq 6$ TeV, so g_B is restricted in the region of $0<g_B\leq 0.85$; (2) The large $\tan\beta$ has been excluded by the

$\overline{B} \to X_s\gamma$ experiment [47,48]. Besides, the Yukawa coupling Y_b is defined as $Y_b = \sqrt{2(\tan\beta^2+1)}m_b/v$. In general, the value of Y_b is smaller than 1, mb $\simeq$ 4.18 GeV and v $\simeq$ 246 GeV, so the parameter $\tan\beta$ should be approximatively smaller than 40; (3) The coupling parameter g_{YB} is taken around -0.45–-0.05, which has been discussed in the works [49,50].

The SM-like Higgs boson mass is $m_h = 125.25 \pm 0.17$ GeV [51–54], which constrains the parameter space strictly. Therefore, we take the suitable parameter space to limit the SM-like Higgs boson mass of the $B-L$ SSM within experimental 4σ, 3σ, and 2σ regions. We also consider the constraints on the NP contribution to the muon MDM in the $B-L$ SSM. The difference between the experimental measurement and SM theoretical prediction of a_μ is $\Delta a_\mu = a_\mu^{\rm exp} - a_\mu^{\rm SM} = (251 \pm 59)\times 10^{-11}$ [51,55], which possesses 4.2σ deviation. Therefore, we constrain the NP contribution $\Delta a_\mu^{\rm NP}$ with 4σ, 3σ, and 2σ experimental errors. Then the numerical results of the CLFV process $l_j^- \to l_i^-\gamma$ are discussed in detail in the following.

A. The CLFV process $\mu \to e\gamma$

We all know that the CLFV process $\mu \to e\gamma$ possesses the strict experimental constraint, so we first discuss this process with $\delta_{13}^{AB} = \delta_{23}^{AB} = 0 (A, B = L, R)$, $\delta_{12}^{LL} = \delta_{12}^{RR} = \delta_{12}^{LR} = 10^{-5}$. Parameters $\tan\beta$, M_1, M_2, μ_H, $M_{BB'}$, $M_{B'}$, $\tilde{A}_e$, $\tilde{m}_L = m_E$, g_{YB}, and g_B are assumed as random variables in the suitable regions. As the SM-like Higgs boson mass and muon MDM are both in 4σ, 3σ, and 2σ regions, and the branching ratio of $\mu \to e\gamma$ satisfies the current experiment constraint, the reasonable parameter space is selected to scatter points which are shown in Fig. 3. Firstly, we discuss the distribution of g_B versus g_{YB} in Fig. 3(a). Under the experimental constraint of 4σ region, the numerical results are mainly concentrated in the upper-right half interval of function $g_B = -2g_{YB}$. In the 3σ interval constraint, the numerical results are mostly located in the region above the function $g_B = -2g_{YB}$ and below the function $g_B = -2g_{YB} + 0.35$. In the 2σ constraint, the numerical results are evenly distributed in the lower-left half interval of the function $g_B = -2g_{YB} + 0.3$, and we find that the region of g_B increases with the decreased g_{YB}, even g_B can be anywhere from 0.2 to 0.85 as $g_{YB} \le -0.25$ with 2σ limit. So g_{YB} takes -0.25 in the following discussion. Besides, in Fig. 3(b), the parameters M_1 and m_E are approximately equal to each other as $\frac{M_{B'}}{m_E} \in (0.9, 1.1)$, and the parameters $M_{B'}$ and m_E are approximately equal to each other when $\frac{M_1}{m_E} \in (0.9, 1.1)$. As the experimental constraint changes from 4σ to 2σ, the values of $\frac{M_{B'}}{m_E}$ and $\frac{M_1}{m_E}$ are both closer to 1. Therefore, in the numerical analyses below, we take $M_1 \simeq 0.947$ TeV, $m_E \simeq 0.948$ TeV, and $M_{B'} \simeq 0.93$ TeV, which are approximately equal to each other. Besides, we appropriately fix $M_2 = 0.6$ TeV, $\mu_H = 0.5$ TeV, and $A_e = 0.4$ TeV to simplify discussion.

The CLFV process $\mu \to e\gamma$ is flavor dependent, which can be influenced by the slepton mixing parameters $\delta_{12}^{AB}(A, B = L, R)$. In order to study the characters of $\delta_{12}^{AB}(A, B = L, R)$ to $\mathrm{Br}(\mu \to e\gamma)$, we assume $g_{YB} = -0.25$, $g_B = 0.8$, $M_{BB'} = 0.8$ TeV, and $\tan\beta = 25$; then the corresponding analyses are shown in Fig. 4. It is obvious that the CLFV rates increase with the enlarged $\delta_{12}^{AB}(A, B = L, R)$ and possess the same changes within 4σ,

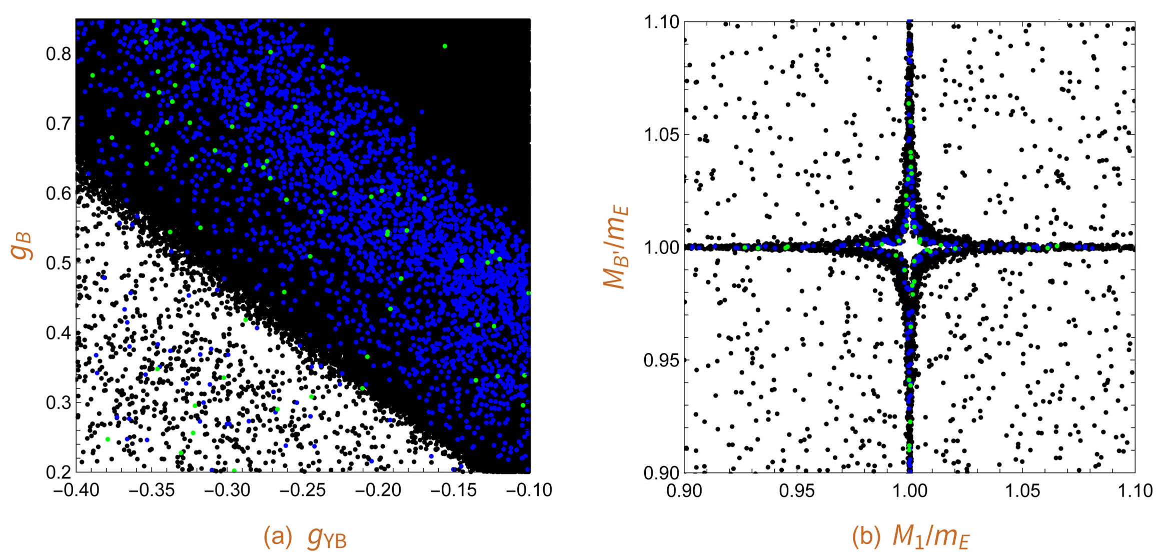

FIG. 3. Under the premise of the limit on the CLFV process $\mu \to e\gamma$, reasonable parameter space is selected to scatter points. Here, the black, blue, and green scatter points correspond to the SM-like Higgs boson mass and muon MDM within 4σ, 3σ, and 2σ regions, respectively.

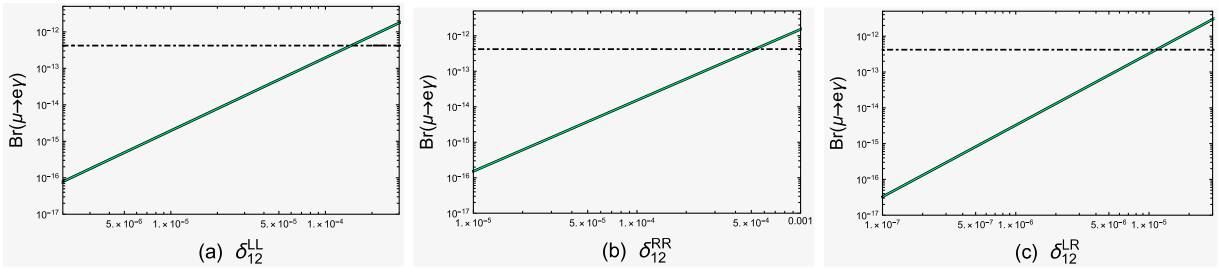

FIG. 4. The CLFV rates for $\mu \to e\gamma$ versus $\delta_{12}^{AB}(A, B = L, R)$, where the dot dashed line denotes the present experimental limit. Here, the black, blue, and green lines correspond to 4σ, 3σ, and 2σ regions, respectively.

3σ, and 2σ constraints. Besides, the present experimental upper bound of $\mathrm{Br}(\mu \to e\gamma)$ constrains $\delta_{12}^{LL} \leq 1.4 \times 10^{-4}$, $\delta_{12}^{RR} \leq 5.1 \times 10^{-4}$, and $\delta_{12}^{LR} \leq 1.1 \times 10^{-5}$.

Then, we study the CLFV rates for $\mu \to e\gamma$ versus g_B, g_{YB}, $M_{BB'}$, and $\tan\beta$ respectively in Fig. 5. In general, the numerical results of $\mathrm{Br}(\mu \to e\gamma)$ enlarge with the increase of g_B, g_{YB}, $M_{BB'}$, and decrease with the increase of $\tan\beta$. The red line has been excluded due to exceeding 4σ experimental constraint of SM-like Higgs mass or muon MDM. And the parameter spaces of g_B, g_{YB}, $M_{BB'}$, and $\tan\beta$ all narrow with the increase of muon MDM and SM-like Higgs mass constraints. Obviously, Figs. 5(a) and 5(b) indicate that the larger g_B or g_{YB} is, the more appropriate CLFV rates for $\mu \to e\gamma$ we can obtain. Under the constraint of 2σ, g_B takes a value in the space of 0.78–0.85 when $g_{YB} = -0.25$ and g_{YB} takes a value in the space of -0.29– -0.25 when $g_B = 0.8$. In Fig. 5(c), when the value of $\tan\beta$ is small, the parameter $M_{BB'}$ can obtain a large region, and the upper and lower limits of $M_{BB'}$ also increase. Furthermore, in the 3σ or 4σ limit, $\tan\beta$ can obtain a larger region—$M_{BB'} = 1.3$ TeV—than that of $M_{BB'} = 0.8$ TeV or $M_{BB'} = 1.8$ TeV. However, in the 2σ region, the space of $\tan\beta$ decreases with the reduced $M_{BB'}$, and even $\tan\beta$ is confined to a much small interval of 22–28 when $M_{BB'} = 0.8$ TeV.

In Refs. [56,57], the authors show that the MIA results can be obtained if one expands the starting expressions in the mass basis properly. The concrete contents include: 1. The loop particles are much heavier than the external states; 2. The convergent of any one-loop amplitude requires that the moduli of every eigenvalue of the dimensionless mass insertion matrix has to be smaller than one, and our discussion satisfies the basic approximation assumption studied in Refs. [56,57]. Besides, we further

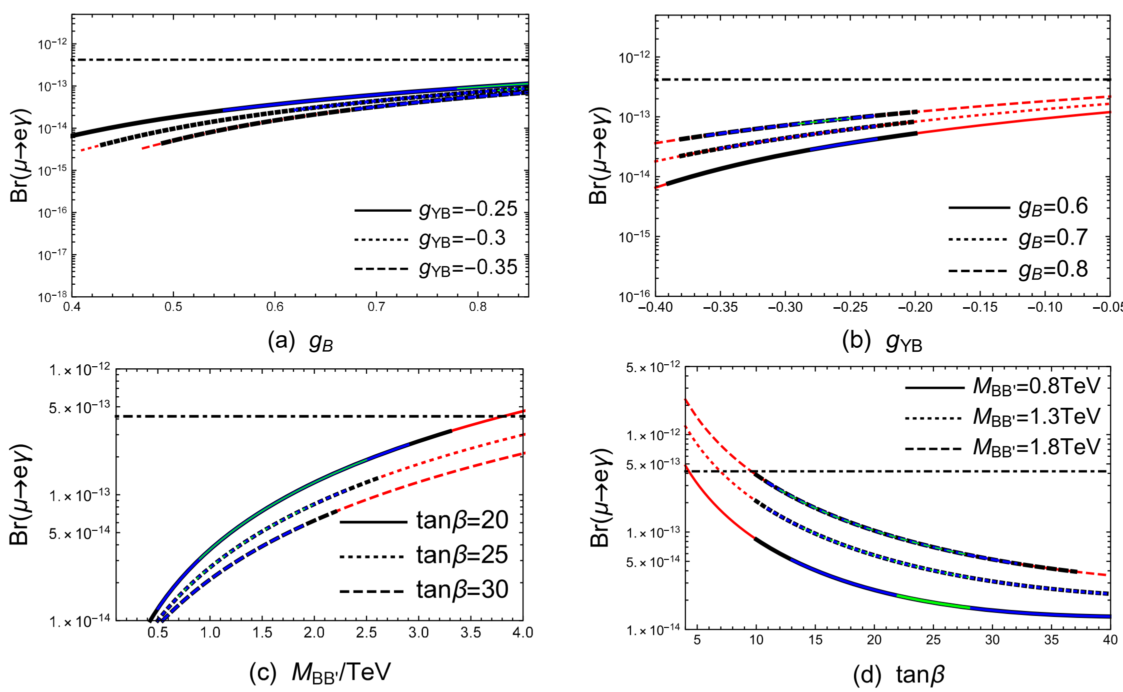

FIG. 5. The $\mathrm{Br}(\mu \to e\gamma)$ versus g_B, g_{YB}, $M_{BB'}$, and $\tan\beta$ respectively, where the dot dashed line denotes the present experimental limit. Here, the black, blue, and green lines correspond to 4σ, 3σ, and 2σ regions, respectively.

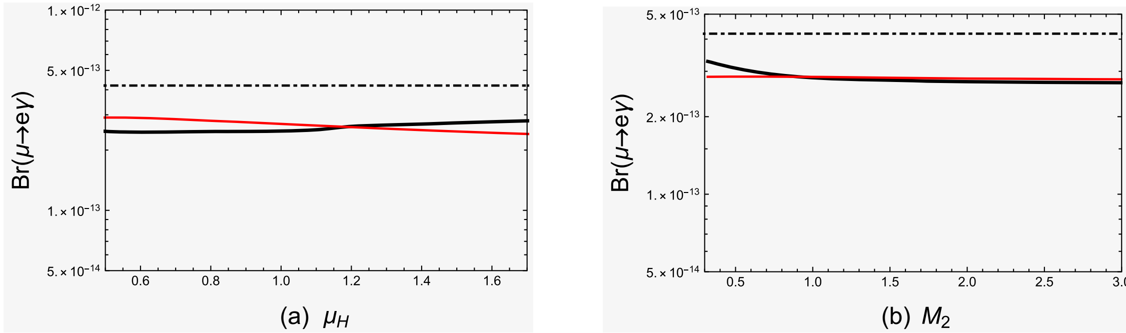

FIG. 6. The CLFV rates for $\mu \to e\gamma$ versus $\mu_H(M_2)$, where the black and red lines correspond to the interaction eigenstate and mass eigenstate, respectively.

study the numerical results of $\mathrm{Br}(\mu \to e\gamma)$ versus $\mu_H(M_2)$ in the interaction eigenstate and mass eigenstate, respectively, in Fig. 6. When parameters are valued in a reasonable space, such as $\delta_{12}^{LL} = 5 \times 10^{-5}$, $\delta_{12}^{RR} = 5 \times 10^{-4}$, $\delta_{12}^{LR} = 9.5 \times 10^{-6}$, $g_{YB} = -0.25$, $g_B = 0.8$, and $\tan\beta = 15$, we find that the $\mathrm{Br}(\mu \to e\gamma)$ with the running of $\mu_H(M_2)$ in the interaction eigenstate have the slight deviation comparing with that in mass eigenstate. Even when μ_H or M_2 takes a certain value, the branch ratios in interaction eigenstate and mass eigenstate are exactly the same. In this work, the numerical discussion of the MIA scheme in the interaction eigenstates is based on satisfying the numerical results of mass eigenstates. Therefore, the compatibility between SARAH and the MIA scheme is guaranteed in this work.

B. The CLFV processes $\tau \to e\gamma$ and $\tau \to \mu\gamma$

Because the experimental upper bounds for $\mathrm{Br}(\tau \to e\gamma)$ and $\mathrm{Br}(\tau \to \mu\gamma)$ do not possess obvious differences, we research both these processes in this section. In Fig. 7, we picture $\mathrm{Br}(\tau \to e\gamma)$ [$\mathrm{Br}(\tau \to \mu\gamma)$] versus the slepton flavor mixing parameters $\delta_{13}^{AB}(A, B = L, R)$ [$\delta_{23}^{AB}(A, B = L, R)$]. Obviously, the CLFV rates of $\tau \to e\gamma$ possess the same trends for 4σ, 3σ, and 2σ limits, as well as $\mathrm{Br}(\tau \to \mu\gamma)$. We can clearly see that all slepton flavor mixing parameters make positive influences on the CLFV rates, even the $\mathrm{Br}(\tau \to e\gamma)$ and $\mathrm{Br}(\tau \to \mu\gamma)$ are respectively proportional to δ_{13}^{AB} and $\delta_{23}^{AB}(A, B = L, R)$. Besides, we find that $\delta_{13}^{LL} \le 0.09$, $\delta_{13}^{RR} \le 0.35$, and $\delta_{13}^{LR} \le 0.13$ with the experimental constraint of $\mathrm{Br}(\tau \to e\gamma)$. Through the present limit of $\mathrm{Br}(\tau \to \mu\gamma)$, δ_{23}^{LL}, δ_{23}^{RR}, and δ_{23}^{LR} are restricted below 0.11, 0.39, and 0.14, respectively.

In order to discuss the effects from other basic parameters on the numerical results, we set $\delta_{13}^{LL} = \delta_{13}^{RR} = \delta_{13}^{LR} = 0.03$ and $\delta_{23}^{AB}(A, B = L, R) = 0$ for process $\tau \to e\gamma$, as well as $\delta_{23}^{LL} = \delta_{23}^{RR} = \delta_{23}^{LR} = 0.03$ and $\delta_{13}^{AB}(A, B = L, R) = 0$ for process $\tau \to \mu\gamma$. Then, we study the influences on $\mathrm{Br}(\tau \to e\gamma)$ and $\mathrm{Br}(\tau \to \mu\gamma)$ from parameters g_B, g_{YB}, $M_{BB'}$, and $\tan\beta$. Overall, the variations of $\mathrm{Br}(\tau \to e\gamma)$ with parameters g_B, g_{YB}, $M_{BB'}$, and $\tan\beta$ are all slightly steeper than that of

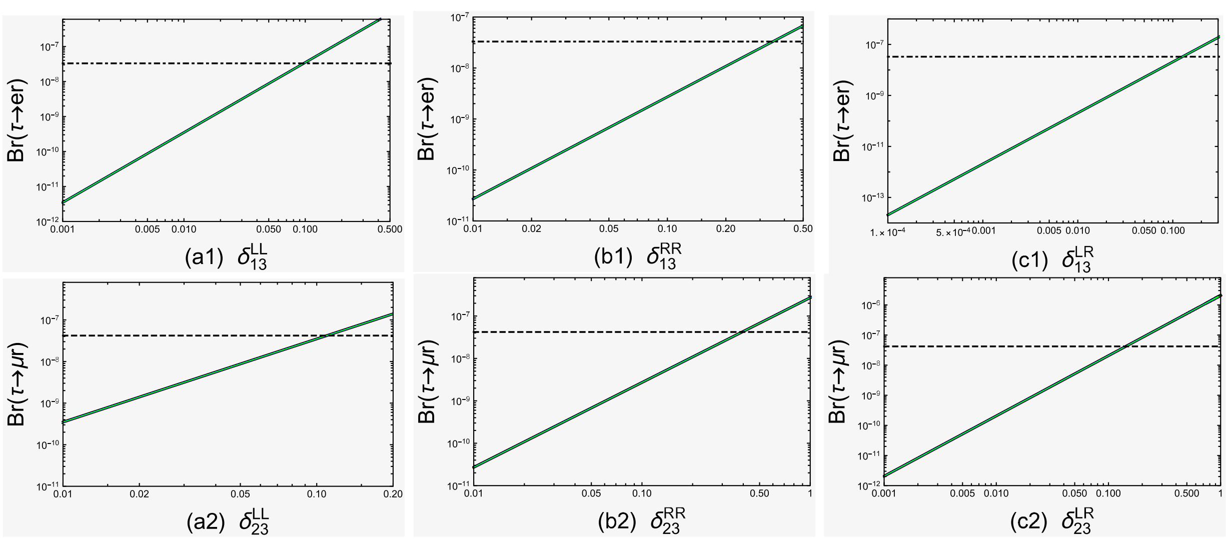

FIG. 7. The CLFV rates for $\tau \to e\gamma(\tau \to \mu\gamma)$ versus $\delta_{13}^{AB}(\delta_{23}^{AB}(A, B = L, R))$, where the dot dashed lines denote the present experimental limits. Here, the black, blue, and green lines correspond to 4σ, 3σ, and 2σ regions, respectively.

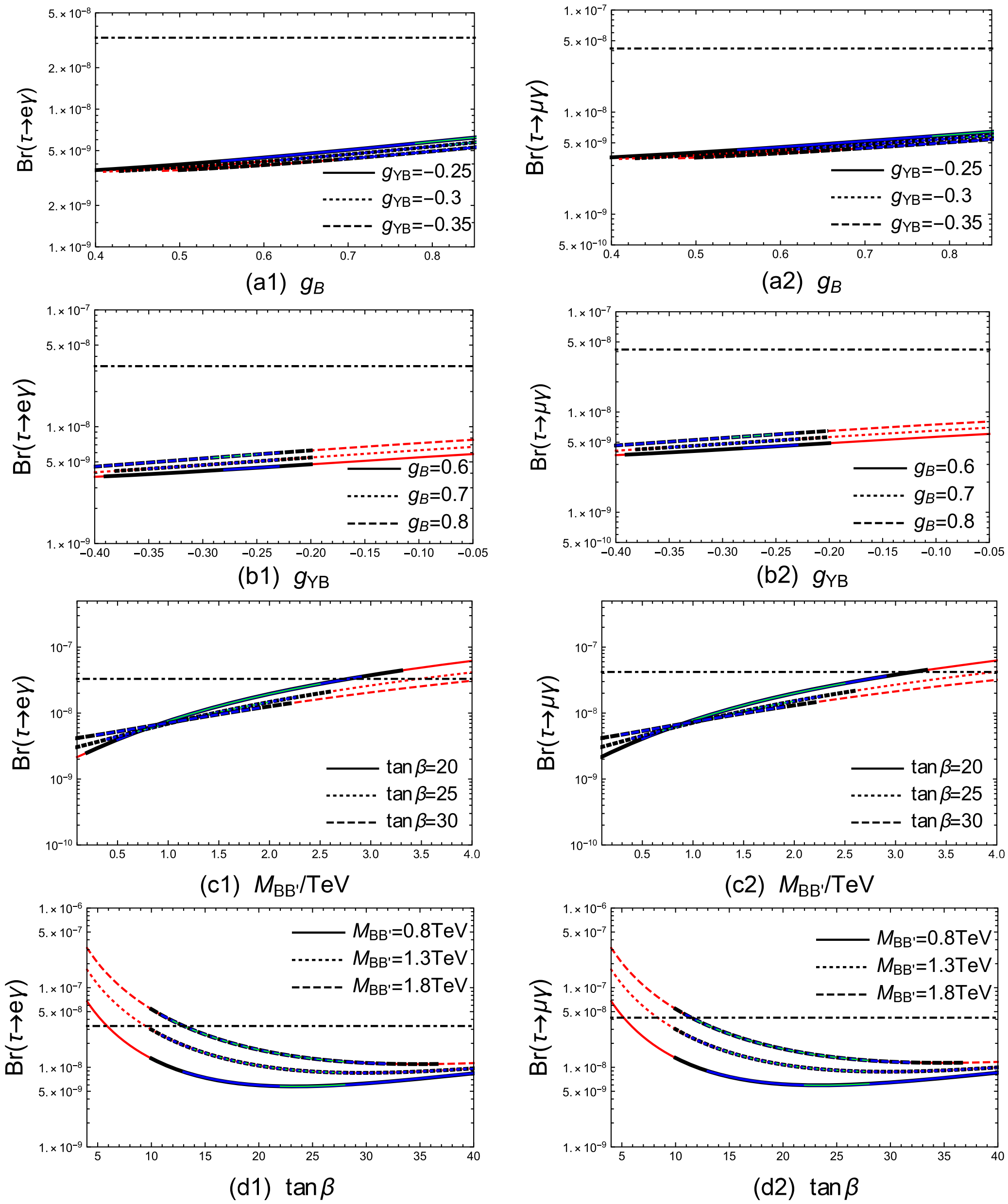

FIG. 8. The CLFV rates change with g_B, g_{YB}, $M_{BB'}$, and $\tan\beta$, where the black, blue, and green lines correspond to 4σ, 3σ, and 2σ regions, and the dot dashed line denotes the experimental limit.

$\mathrm{Br}(\tau \to \mu\gamma)$, and the value spaces of g_B, g_{YB}, $M_{BB'}$, and $\tan\beta$ become small as the constraints of SM-like Higgs mass and muon MDM change from 4σ to 2σ. Figures 8(a1) and 8(a2) both indicate that the ranges of g_B increase as g_{YB} expands, and when $g_{YB} = -0.25$, g_B can fetch all values from 0.78 to 0.85 under the 2σ constraint. g_{YB} in Figs. 8(b1) and 8(b2) can both obtain smallest regions when $g_B = 0.7$ with the limits of 4σ. However, within 3σ limit, the larger g_B is, the larger space for reasonable values g_{YB} is. Under the 2σ constraint, g_{YB} runs in a -0.29–-0.25 cell only when $g_B = 0.8$.

In Figs. 8(c1) and 8(c2), we can see that the large regions of $M_{BB'}$ have been eliminated by the experimental upper limits of $\mathrm{Br}(\tau \to e\gamma)$ and $\mathrm{Br}(\tau \to \mu\gamma)$ both within the 4σ or 3σ limit, but $M_{BB'}$ can still obtain large region as $\tan\beta = 20$. Besides, the experimental limit of $\mathrm{Br}(\tau \to e\gamma)$ is stronger than that of $\mathrm{Br}(\tau \to \mu\gamma)$. Under the constraint of 2σ, the value range of $M_{BB'}$ changes from 0.7 TeV to 2 TeV as $\tan\beta = 25$, which is more narrow than that of $\tan\beta = 20$ (here 0.9 TeV $\leq M_{BB'} \leq$ 2.5 TeV). In addition, considering 4σ or 3σ constraint on the Figs. 8(d1) and 8(d2), we find that the larger $M_{BB'}$ is, the more obvious experimental constraints of $\mathrm{Br}(\tau\to e\gamma)$ and $\mathrm{Br}(\tau\to\mu\gamma)$ on $\tan\beta$ are, and the smaller value space of $\tan\beta$ is. That is to say the suitable parameter space of $\tan\beta$ narrows obviously as $M_{BB'}$ enlarges. When $M_{BB'}=1.8$ TeV, $\tan\beta$ can be any value between 14 and 28 within the 2σ region, which indicates parameter $\tan\beta$ is more constrained by the experimental limit of $\mathrm{Br}(\tau\to e\gamma)$ than $\mathrm{Br}(\tau\to\mu\gamma)$.

V. DISCUSSION AND CONCLUSION

In this work, under the premise that the compatibility between SARAH and the MIA scheme is guaranteed, we focus on CLFV processes $l_j^-\to l_i^-\gamma$ in the $B-L$ SSM using the MIA method. Assuming that all superparticle masses are almost degenerate, we find that the $B-L$ SSM contributions for both muon MDM and CLFV processes beyond MSSM are considerable at the analytical level. In the numerical discussion, we constrain the SM-like Higgs mass and muon MDM both within the 4σ, 3σ, and 2σ regions, which possess strict limits on the CLFV decays. Firstly, the distribution of g_B versus g_{YB} presents different sensitive parameter regions under the different bounds within 2σ, 3σ, and 4σ. Besides, the parameters M_1 and m_E are approximately equal to each other as $\frac{M_{B'}}{m_E}\in(0.9,1.1)$, as well as the parameters $M_{B'}$ and m_E being approximately equal to each other when $\frac{M_1}{m_E}\in(0.9,1.1)$. As the experimental constraint changes from 4σ to 2σ, the values of $\frac{M_{B'}}{m_E}$ and $\frac{M_1}{m_E}$ are both closer to 1. The branching ratios of $l_j^-\to l_i^-\gamma$ depend on the slepton flavor mixing parameters δ_{12}^{AB}, δ_{13}^{AB}, and $\delta_{23}^{AB}(A,B=L,R)$ obviously, and $\mathrm{Br}(l_j^-\to l_i^-\gamma)$ increases with the enlarged δ_{12}^{AB}, δ_{13}^{AB}, and δ_{23}^{AB}. Considering the latest experimental limits of $\mathrm{Br}(l_j^-\to l_i^-\gamma)$, the slepton flavor mixing parameters are restricted as $\delta_{12}^{LL}\le 1.4\times10^{-4}$, $\delta_{12}^{RR}\le 5.1\times10^{-4}$, $\delta_{12}^{LR}\le 1.1\times10^{-5}$, $\delta_{13}^{LL}\le 0.09$, $\delta_{13}^{RR}\le 0.35$, $\delta_{13}^{LR}\le 0.13$, $\delta_{23}^{LL}\le 0.11$, and $\delta_{23}^{RR}\le 0.39$ and $\delta_{23}^{LR}\le 0.14$.

The parameter ranges of g_B, g_{YB}, $M_{BB'}$, and $\tan\beta$ all narrow obviously as the constraints of SM-like Higgs mass and muon MDM change from 4σ to 2σ. Compared with the MSSM, g_B, g_{YB}, and $M_{BB'}$ are the new parameters in the $B-L$ SSM, which have an uplift effects on the numerical results. At 3σ or 2σ limit, g_B has a large region with the increased g_{YB}, similarly, the reasonable parameter space of g_{YB} also widens as the value of g_B enlarges. When $g_{YB}=-0.25(g_B=0.8)$, $g_B(g_{YB})$ is constrained in the range of 0.78–0.85(−0.29– − 0.25), which corresponds to the maximum spaces of these parameters under the 2σ constraint. Under the 2σ constraint, the parameter $M_{BB'}$ can obtain a large reasonable space 0.9–2.5 TeV when $\tan\beta=20$. The large parameter space of $\tan\beta$ is excluded by the latest experiment limit of $\mathrm{Br}(\tau\to e\gamma)$, which possesses the strongest constraint. Therefore, under the 2σ and $\mathrm{Br}(\tau\to e\gamma)$ constraints, $\tan\beta$ can run in a much large region of 14–28 when $M_{BB'}=1.8$ TeV.

ACKNOWLEDGMENTS

This work is supported by the Major Project of National Natural Science Foundation of China (NNSFC) (No. 12235008), the National Natural Science Foundation of China (NNSFC) (No. 12075074, No. 12075073), the Natural Science Foundation of Hebei province (No. A2022201022, No. A2020201002 and No. A2023201041), the Foundation of Hebei Education Department (No. QN2022173).

APPENDIX A: ONE-LOOP FUNCTIONS

The one-loop functions $\mathcal{I}(x,y,z)$, $\mathcal{J}(x,y,z)$, $f(x,y,z,t)$, $g(x,y,z,t)$, and $k(x,y,z,t)$ can be written as

$$\mathcal{I}(x,y,z)=\frac{1}{16\pi^2}\left[\frac{1}{(x-z)(z-y)}+\frac{(z^2-xy)\log z}{(x-z)^2(y-z)^2}-\frac{x\log x}{(x-y)(x-z)^2}+\frac{y\log y}{(x-y)(y-z)^2}\right],$$

$$\mathcal{J}(x,y,z)=\frac{1}{16\pi^2}\left[\frac{x(x^2+xz-2yz)\log x}{(x-y)^2(x-z)^3}-\frac{y^2\log y}{(x-y)^2(y-z)^2}+\frac{z[x(z-2y)+z^2]\log z}{(z-x)^3(y-z)^2}-\frac{x(y-2z)+yz}{(x-y)(x-z)^2(y-z)}\right],$$

$$\begin{aligned}f(x,y,z,t)=\frac{1}{16\pi^2}&\left[\frac{t[t^3-3txy+xy(x+y)]\log t}{(t-x)^3(t-y)^3(t-z)}-\frac{x[x^3-3txz+tz(t+z)]\log x}{(t-x)^3(x-y)(x-z)^3}\right.\\&+\frac{y[y^3-3tyz+tz(t+z)]\log y}{(t-y)^3(x-y)(y-z)^3}-\frac{z[z^3-3xyz+xy(x+y)]\log z}{(t-z)(z-x)^3(z-y)^3}+\frac{1}{2(x-y)}\\&\left.\times\left(\frac{t}{(t-x)^2(z-x)}-\frac{2y}{(t-y)(y-z)^2}+\frac{x(2t-3x+z)}{(t-x)^2(x-z)^2}+\frac{t+y}{(t-y)^2(y-z)}\right)\right],\end{aligned}$$

$$
\begin{aligned}
g(x,y,z,t) = \frac{1}{16\pi^2}\Big\{ & -\frac{t[t^3(x+y)-3t^2xy+x^2y^2]\log t}{(t-x)^3(t-y)^3(t-z)} + \frac{z[x^2y^2+xz^2(z-3y)+yz^3]\log z}{(t-z)(z-x)^3(z-y)^3} \\
& + \frac{x^2[x^3-3txz+tz(t+z)]\log x}{(t-x)^3(x-y)(x-z)^3} - \frac{y^2[y^3-3tyz+tz(t+z)]\log y}{(t-y)^3(x-y)(y-z)^3} - \frac{x^2(2t-3x+z)}{2(t-x)^2(x-y)(x-z)^2} \\
& + \frac{tx}{2(t-x)^2(x-y)(x-z)} - \frac{y[t(y+z)+y(z-3y)]}{2(t-y)^2(y-x)(y-z)^2}\Big\}, \\
k(x,y,z,t) = \frac{1}{16\pi^2}\Big\{ & -\frac{[z(x^2-ty)+x^2(t-2x+y)]\log x}{(t-x)^2(x-y)^2(x-z)^2} - \frac{t\log t}{(t-x)^2(t-y)(t-z)} \\
& + \frac{y\log y}{(t-y)(x-y)^2(y-z)} + \frac{1}{(t-x)(x-y)(x-z)} + \frac{z\log z}{(t-z)(z-y)(x-z)^2}\Big\}. \qquad \text{(A1)}
\end{aligned}
$$

APPENDIX B: THE CHIRALITY FLIPS

The chirality flips occurring in the internal gaugino and the external lepton lines were described in detail in the Refs. [58–60]. Since the gaugino mass is much bigger than the lepton mass, these diagrams whose chirality flips occur in the internal gaugino lines may yield dominant contributions.

Then, we take two Feynman pictures shown in Fig. 9 as the examples, and discuss the chirality flips occurring in the internal gaugino and the external lepton lines as follows. Firstly, we discuss the concrete amplitude of Fig. 9(a),

$$
\begin{aligned}
i\mathcal{M}_1 = \bar{u}_i(p+q)\mu^{4-D}\int\frac{d^Dk}{(2\pi)^D}\Bigg[& \frac{eA_LP_L(\not{k}+M_1)B_LP_L(2p+q-2k)^\mu C}{[k^2-M_1^2][(k-p)^2-m^2_{\tilde{L}^L_j}][(k-(p+q))^2-m^2_{\tilde{L}^L_j}][(k-(p+q))^2-m^2_{\tilde{L}^R_i}]} \\
& + \frac{eA_LP_L(\not{k}+M_1)B_LP_L(2p+q-2k)^\mu C}{[k^2-M_1^2][(k-p)^2-m^2_{\tilde{L}^L_j}][(k-p)^2-m^2_{\tilde{L}^R_i}][(k-(p+q))^2-m^2_{\tilde{L}^R_i}]}\Bigg]u_j(p)\epsilon_\mu(q). \qquad \text{(B1)}
\end{aligned}
$$

We assume that the internal masses of particles such as gaugino and left(right)-handed slepton are much bigger than the external lepton mass, the function $\frac{1}{(k-p)^2-m^2} \simeq \frac{1}{k^2-m^2} + \frac{2k\cdot p-p^2}{(k^2-m^2)^2} + \frac{4(k\cdot p)^2}{(k^2-m^2)3}$. Then the amplitude can be approximately reduced as

$$
\begin{aligned}
i\mathcal{M}_1 \simeq \bar{u}_i(p+q)eM_1CA_LB_LP_L\mu^{4-D}\int & \frac{d^Dk}{(2\pi)^D}\frac{(2p+q)^\mu}{[k^2-M_1^2][k^2-m^2_{\tilde{L}^L_j}][k^2-m^2_{\tilde{L}^R_i}]}\Bigg[\frac{1}{k^2-m^2_{\tilde{L}^L_j}} \\
& + \frac{1}{k^2-m^2_{\tilde{L}^R_i}} - \frac{k^2}{(k^2-m^2_{\tilde{L}^L_j})^2} - \frac{k^2}{(k^2-m^2_{\tilde{L}^R_i})^2} - \frac{k^2}{(k^2-m^2_{\tilde{L}^L_j})(k^2-m^2_{\tilde{L}^R_i})}\Bigg]u_j(p)\epsilon_\mu(q) \\
= -\bar{u}_i(p+q)eM_1CA_LB_LP_Li\sigma^{\mu\nu}q_\nu & \frac{i}{2\Lambda^4}[\mathcal{J}(x_1,x_{\tilde{L}^L_j},x_{\tilde{L}^R_i}) + \mathcal{J}(x_1,x_{\tilde{L}^R_i},x_{\tilde{L}^L_j})]u_j(p)\epsilon_\mu(q). \qquad \text{(B2)}
\end{aligned}
$$

With $A_L = -\sqrt{2}g_1$, $B_L = \frac{g_1}{\sqrt{2}}$ and $C = -\triangle^{LR}_{ij} = -A_ev_d\delta^{LR}_{ij}$, the Wilson coefficient of Fig. 9(a) can be written as

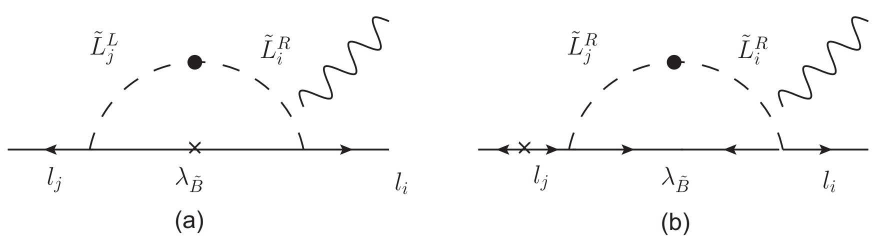

FIG. 9. The Feynman diagrams of $l_j^- \to l_i^-\gamma$ by MIA in the B-LSSM, the chirality flips occur in the internal gaugino and external lepton lines, respectively.

$$C_2(\tilde{L}_j^L, \tilde{L}_i^R, \lambda_{\tilde{B}}) = -\frac{g_1^2}{2\Lambda^4 m_{l_j}} M_1 A_e v_d \delta_{ij}^{LR} P_L[\mathcal{J}(x_1, x_{\tilde{L}_j^L}, x_{\tilde{L}_i^R}) + \mathcal{J}(x_1, x_{\tilde{L}_i^R}, x_{\tilde{L}_j^L})]. \tag{B3}$$

Here, the chirality flip occurs in the internal gaugino line.

Secondly, we take Fig. 9(b) as an example, and discuss the chirality flip occurs in the external lepton line. The concrete amplitude is written as

$$\begin{aligned}
i\mathcal{M}_2 &= \bar{u}_i(p+q)\mu^{4-D}\int\frac{d^Dk}{(2\pi)^D}\left[\frac{eA_LP_L(\not{k}+M_1)B_RP_R(2p+q-2k)^\mu C'}{[k^2-M_1^2][(k-p)^2-m_{\tilde{L}_j^R}^2][(k-(p+q))^2-m_{\tilde{L}_j^R}^2][(k-(p+q))^2-m_{\tilde{L}_i^R}^2]}\right.\\
&\quad\left.+\frac{eA_LP_L(\not{k}+M_1)B_RP_R(2p+q-2k)^\mu C'}{[k^2-M_1^2][(k-p)^2-m_{\tilde{L}_j^R}^2][(k-p)^2-m_{\tilde{L}_i^R}^2][(k-(p+q))^2-m_{\tilde{L}_i^R}^2]}\right]u_j(p)\epsilon_\mu(q)\\
&\simeq \bar{u}_i(p+q)eC'A_LB_RP_L\mu^{4-D}\int\frac{d^Dk}{(2\pi)^D}\frac{\not{k}(2p+q)^\mu 2k\cdot(2p+q)}{[k^2-M_1^2][k^2-m_{\tilde{L}_j^R}^2][k^2-m_{\tilde{L}_i^R}^2]}\left[\frac{1}{(k^2-m_{\tilde{L}_j^R}^2)^2}\right.\\
&\quad\left.+\frac{1}{(k^2-m_{\tilde{L}_j^R}^2)(k^2-m_{\tilde{L}_i^R}^2)}+\frac{1}{(k^2-m_{\tilde{L}_i^R}^2)^2}\right]u_j(p)\epsilon_\mu(q)\\
&\simeq \bar{u}_i(p+q)eC'A_LB_RP_L\mu^{4-D}\int\frac{d^Dk}{(2\pi)^D}\frac{1}{2}\frac{(2p+q)^\mu(2\not{p}+\not{q})}{[k^2-M_1^2][k^2-m_{\tilde{L}_j^R}^2][k^2-m_{\tilde{L}_i^R}^2]}\left[\frac{k^2}{(k^2-m_{\tilde{L}_j^R}^2)^2}\right.\\
&\quad\left.+\frac{k^2}{(k^2-m_{\tilde{L}_j^R}^2)(k^2-m_{\tilde{L}_i^R}^2)}+\frac{k^2}{(k^2-m_{\tilde{L}_i^R}^2)^2}\right]u_j(p)\epsilon_\mu(q)\\
&= -\bar{u}_i(p+q)eC'A_LB_R\left(\frac{m_{l_j}}{2}P_L+\frac{m_{l_i}}{2}P_R\right)i\sigma^{\mu\nu}q_\nu\frac{i}{2\Lambda^4}[2\mathcal{I}(x_{\tilde{L}_j^R},x_1,x_{\tilde{L}_i^R})\\
&\quad+2\mathcal{I}(x_{\tilde{L}_i^R},x_1,x_{\tilde{L}_j^R})-\mathcal{J}(x_{\tilde{L}_j^R},x_{\tilde{L}_i^R},x_1)-\mathcal{J}(x_{\tilde{L}_i^R},x_{\tilde{L}_j^R},x_1)]u_j(p)\epsilon_\mu(q).
\end{aligned} \tag{B4}$$

With $A_L = B_R = -\sqrt{2}g_1$, $C' = -\triangle_{ij}^{RR} = -m_E^2\delta_{ij}^{RR}$, and $m_{l_j} \gg m_{l_i}$, the Wilson coefficient of Fig. 9(b) can be written as

$$C_2'(\tilde{L}_j^R, \tilde{L}_i^R, \lambda_{\tilde{B}}) \simeq \frac{g_1^2}{2\Lambda^4} m_E^2 \delta_{ij}^{RR} P_L\left[2\mathcal{I}(x_{\tilde{L}_j^R}, x_1, x_{\tilde{L}_i^R}) + 2\mathcal{I}(x_{\tilde{L}_i^R}, x_1, x_{\tilde{L}_j^R}) - \mathcal{J}(x_{\tilde{L}_j^R}, x_{\tilde{L}_i^R}, x_1) - \mathcal{J}(x_{\tilde{L}_i^R}, x_{\tilde{L}_j^R}, x_1)\right]. \tag{B5}$$

If $|M_1| = m_L = m_E = A_e = \Lambda$, then $C_2(\tilde{L}_j^L, \tilde{L}_i^R, \lambda_{\tilde{B}}) \to -\frac{g_1^2}{192\pi^2\Lambda^4 m_{l_j}} M_1 A_e v_d \delta_{ij}^{LR} P_L$, and $C_2'(\tilde{L}_j^R, \tilde{L}_i^R, \lambda_{\tilde{B}}) \to \frac{g_1^2}{64\pi^2\Lambda^4 m_{l_j}} m_{l_j} m_E^2 \delta_{ij}^{RR} P_L$. If δ_{ij}^{RR} and δ_{ij}^{LR} in the same order, $M_1 A_e v_d \gg m_{l_j} m_E^2$, then the absolute value of $C_2(\tilde{L}_j^L, \tilde{L}_i^R, \lambda_{\tilde{B}})$ is much bigger than $C_2'(\tilde{L}_j^R, \tilde{L}_i^R, \lambda_{\tilde{B}})$. Therefore, we omit the chirality flip of incident lepton in our calculation.

APPENDIX C: THE COMPARISONS FROM FIGS. 2(a1) AND (a2)

We now discuss the one-loop contributions from $\tilde{H}^- - \tilde{W}^- - \tilde{\nu}_L^R$ in detail, which is derived from Fig. 2(a1). The concrete amplitude is

$$\begin{aligned}
i\mathcal{M}_{a1} &= \bar{u}_i(p+q)\int\frac{d^4k}{(2\pi)^D}\left[\frac{eA_LP_L(\not{k}+\not{p}+\not{q}+\mu_H)(B_LP_L+B_RP_R)(\not{k}+\not{p}+\not{q}+M_2)\gamma^\mu(\not{k}+\not{p}+M_2)C_LP_LD}{[(k+p+q)^2-\mu_H^2][(k+p+q)^2-M_2^2][(k+p)^2-M_2^2][k^2-m_{\tilde{\nu}_{L_j}^R}^2][k^2-m_{\tilde{\nu}_{L_i}^R}^2]}\right.\\
&\quad\left.+\frac{eA_LP_L(\not{k}+\not{p}+\not{q}+\mu_H)\gamma^\mu(\not{k}+\not{p}+\mu_H)(B_LP_L+B_RP_R)(\not{k}+\not{p}+M_2)C_LP_LD}{[(k+p+q)^2-\mu_H^2][(k+p)^2-\mu_H^2][(k+p)^2-M_2^2][k^2-m_{\tilde{\nu}_{L_j}^R}^2][k^2-m_{\tilde{\nu}_{L_i}^R}^2]}\right]u_j(p)\epsilon_\mu(q).
\end{aligned} \tag{C1}$$

We assume that the internal masses of particles are much bigger than the external lepton mass, the function $\frac{1}{(k+p)^2-m^2} \simeq \frac{1}{k^2-m^2} - \frac{2k\cdot p+p^2}{(k^2-m^2)^2} + \frac{4(k\cdot p)^2}{(k^2-m^2)3}$. With $A_L = \frac{Y_{l_i}}{\sqrt{2}}$, $B_L = -\frac{g_2}{\sqrt{2}}v_d\tan\beta$, $B_R = -\frac{g_2}{\sqrt{2}}v_d$ (here $B_L \gg B_R$), $C_L = \frac{g_2}{\sqrt{2}}$ and $D = -\triangle_{ij}^{LL}$, then the amplitude can be approximately reduced as

$$
\begin{aligned}
i\mathcal{M}_{a1} \simeq & -\bar{u}_i(p+q)\int\frac{d^4k}{(2\pi)^D}\frac{e\mu_H M_2 A_L B_L C_L D P_L (2p+q)^\mu}{[k^2-\mu_H^2][k^2-M_2^2][k^2-m^2_{\tilde{\nu}^R_{L_j}}][k^2-m^2_{\tilde{\nu}^R_{L_i}}]}\\
&\times\left[\frac{k^2}{(k^2-\mu_H^2)^2}+\frac{k^2}{(k^2-M_2^2)^2}+\frac{k^2}{(k^2-\mu_H^2)(k^2-M_2^2)}\right]u_j(p)\epsilon_\mu(q)\\
= & \, i\bar{u}_i(p+q)em_{l_j}i\sigma^{\mu\nu}q_\nu\frac{g_2^2}{2\Lambda^4}\frac{m_{l_i}}{m_{l_j}}\sqrt{x_2 x_{\mu_H}}\Delta^{LL}_{ij}\tan\beta[k(x_{\mu_H},x_2,x_{\tilde{\nu}^R_{L_j}},x_{\tilde{\nu}^R_{L_i}})\\
&+k(x_2,x_{\mu_H},x_{\tilde{\nu}^R_{L_j}},x_{\tilde{\nu}^R_{L_i}})-f(x_2,x_{\mu_H},x_{\tilde{\nu}^R_{L_j}},x_{\tilde{\nu}^R_{L_i}})]P_L u_j(p)\epsilon_\mu(q). \qquad \text{(C2)}
\end{aligned}
$$

Using the same method with Fig. 2(a1), the concrete amplitude of Fig. 2(a2) can be written as

$$
\begin{aligned}
i\mathcal{M}_{a2} = \bar{u}_i(p+q)\int\frac{d^4k}{(2\pi)^D}\Bigg[&\frac{eA'_R P_R(\not{k}+\not{p}+\not{q}+M_2)(B'_L P_L+B'_R P_R)(\not{k}+\not{p}+\not{q}+\mu_H)\gamma^\mu(\not{k}+\not{p}+\mu_H)C'_R P_R D}{[(k+p+q)^2-M_2^2][(k+p+q)^2-\mu_H^2][(k+p)^2-\mu_H^2][k^2-m^2_{\tilde{\nu}^R_{L_j}}][k^2-m^2_{\tilde{\nu}^R_{L_i}}]}\\
&+\frac{eA'_R P_R(\not{k}+\not{p}+\not{q}+M_2)\gamma^\mu(\not{k}+\not{p}+M_2)(B'_L P_L+B'_R P_R)(\not{k}+\not{p}+\mu_H)C'_R P_R D}{[(k+p+q)^2-M_2^2][(k+p)^2-M_2^2][(k+p)^2-\mu_H^2][k^2-m^2_{\tilde{\nu}^R_{L_j}}][k^2-m^2_{\tilde{\nu}^R_{L_i}}]}\Bigg]u_j(p)\epsilon_\mu(q). \qquad \text{(C3)}
\end{aligned}
$$

With $A'_R=\frac{g_2}{\sqrt{2}}$, $B'_L=-\frac{g_2}{\sqrt{2}}v_d$, $B'_R=-\frac{g_2}{\sqrt{2}}v_d\tan\beta$ (here $B'_L \ll B'_R$), $C'_R=\frac{Y_{l_j}}{\sqrt{2}}$, and $D=-\triangle^{LL}_{ij}$, then the amplitude can be approximately reduced as

$$
\begin{aligned}
i\mathcal{M}_{a2} \simeq & -\bar{u}_i(p+q)\int\frac{d^4k}{(2\pi)^D}\frac{e\mu_H M_2 A'_R B'_R C'_R D P_R (2p+q)^\mu}{[k^2-\mu_H^2][k^2-M_2^2][k^2-m^2_{\tilde{\nu}^R_{L_j}}][k^2-m^2_{\tilde{\nu}^R_{L_i}}]}\\
&\times\left[\frac{k^2}{(k^2-\mu_H^2)^2}+\frac{k^2}{(k^2-M_2^2)^2}+\frac{k^2}{(k^2-\mu_H^2)(k^2-M_2^2)}\right]u_j(p)\epsilon_\mu(q)\\
= & \, i\bar{u}_i(p+q)em_{l_j}i\sigma^{\mu\nu}q_\nu\frac{g_2^2}{2\Lambda^4}\sqrt{x_2 x_{\mu_H}}\Delta^{LL}_{ij}\tan\beta[k(x_{\mu_H},x_2,x_{\tilde{\nu}^R_{L_j}},x_{\tilde{\nu}^R_{L_i}})\\
&+k(x_2,x_{\mu_H},x_{\tilde{\nu}^R_{L_j}},x_{\tilde{\nu}^R_{L_i}})-f(x_2,x_{\mu_H},x_{\tilde{\nu}^R_{L_j}},x_{\tilde{\nu}^R_{L_i}})]P_R u_j(p)\epsilon_\mu(q). \qquad \text{(C4)}
\end{aligned}
$$

Therefore, in the one-loop contribution from $\tilde{H}^- - \tilde{W}^- - \tilde{\nu}^R_L$, the term including the incident lepton is dominant.

---

[1] S. T. Petcov, Sov. J. Nucl. Phys. **25**, 340 (1977).
[2] A. M. Baldini *et al.* (MEG Collaboration), Eur. Phys. J. C **76**, 434 (2016).
[3] B. Aubert *et al.* (*BABAR* Collaboration), Phys. Rev. Lett. **104**, 021802 (2010).
[4] K. Uno *et al.* (BELLE Collaboration), J. High Energy Phys. 10 (2021) 019.
[5] A. Ilakovac and A. Pilaftsis, Nucl. Phys. **B437**, 491 (1995).
[6] R. Diaz, R. Martinez, and J. A. Rodriguez, Phys. Rev. D **63**, 095007 (2001).
[7] M. Kakizaki, Y. Ogura, and F. Shima, Phys. Lett. B **566**, 210 (2003).
[8] E. Arganda and M. J. Herrero, Phys. Rev. D **73**, 055003 (2006).
[9] T. Toma and A. Vicente, J. High Energy Phys. 01 (2014) 160.
[10] H. B. Zhang, T. F. Feng, S. M. Zhao, and F. Sun, Int. J. Mod. Phys. A **29**, 1450123 (2014).
[11] S. M. Zhao, T. F. Feng, H. B. Zhang, X.-J. Zhan, Y.-J. Zhang, and B. Yan, Phys. Rev. D **92**, 115016 (2015).
[12] J. L. Yang, T. F. Feng, Y. L. Yan, W. Li, S.-M. Zhao, and H.-B. Zhang, Phys. Rev. D **99**, 015002 (2019).
[13] T. Nomura, H. Okada, and Y. Uesaka, Nucl. Phys. **B962**, 115236 (2021).
[14] V. Barger, P. F. Perez, and S. Spinner, Phys. Rev. Lett. **102**, 181802 (2009).
[15] P. F. Perez and S. Spinner, Phys. Lett. B **673**, 251 (2009).
[16] M. Ambroso and B. A. Ovrut, Int. J. Mod. Phys. A **26**, 1569 (2011).
[17] P. F. Perez and S. Spinner, Phys. Rev. D **83**, 035004 (2011).
[18] J. L. Yang, S. M. Zhao, R. F. Zhu, X.-Y. Yang, and H.-B. Zhang, Eur. Phys. J. C **78**, 714 (2018).

[19] T. Moroi, Phys. Rev. D **53**, 6565 (1996).
[20] E. Arganda, M. J. Herrero, R. Morales, and A. Szynkman, J. High Energy Phys. 03 (2016) 055.
[21] E. Arganda, M. J. Herrero, X. Marcano R. Morales, and A. Szynkman, Phys. Rev. D **95**, 095029 (2017).
[22] M. J. Herrero, X. Marcano, R. Morales, and A. Szynkman, Eur. Phys. J. C **78**, 815 (2018).
[23] S. M. Zhao, L. H. Su, X. X. Dong, T.-T. Wang, and T.-F. Feng, J. High Energy Phys. 03 (2022) 101.
[24] T. T. Wang, S. M. Zhao, J. F. Zhang, X.-X. Dong, and T.-F. Feng, Eur. Phys. J. C **82**, 639 (2022).
[25] H. P. Nilles, Phys. Rep. **110**, 1 (1984).
[26] H. E. Haber and G. L. Kane, Phys. Rep. **117**, 75 (1985).
[27] J. Rosiek, Phys. Rev. D **41**, 3464 (1990).
[28] T. F. Feng and X. Y. Yang, Nucl. Phys. **B814**, 101 (2009).
[29] C. S. Aulakh, A. Melfo, A. Rasin, and G. Senjanovic, Phys. Lett. B **459**, 557 (1999).
[30] W. Abdallah, A. Hammad, S. Khalil, and S. Moretti, Phys. Rev. D **95**, 055019 (2017).
[31] J. L. Yang, T. F. Feng, and H. B. Zhang, Eur. Phys. J. C **80**, 210 (2020).
[32] S. Khalil and H. Okada, Phys. Rev. D **79**, 083510 (2009).
[33] L. Basso, B. O'Leary, W. Porod, and F. Staub, J. High Energy Phys. 09 (2012) 054.
[34] L. D. Rose, S. Khalil, S. J. D. King, C. Marzo, S. Moretti, and C. S. Un, Phys. Rev. D **96**, 055004 (2017).
[35] L. D. Rose, S. Khalil, S. J. D. King, S. Kulkarni, C. Marzo, S. Moretti, and C. S. Un, J. High Energy Phys. 07 (2018) 100.
[36] P. H. Chankowski, S. Pokorski, and J. Wagner, Eur. Phys. J. C **47**, 187 (2006).
[37] F. Staub, Adv. Ser. Dir. High Energy Phys. **2015**, 840780 (2015).
[38] F. Staub, arXiv:0806.0538.
[39] M. Carena, J. R. Espinosaos, C. E. M. Wagner, Phys. Lett. B **355**, 209 (1995).
[40] M. Carena, M. Quiros, and C. E. M. Wagner, Nucl. Phys. **B461**, 407 (1996).
[41] M. Carena, S. Gori, N. R. Shah, and C. E. M. Wagner, J. High Energy Phys. 03 (2012) 014.
[42] T. F. Feng, L. Sun, and X. Y. Yang, Nucl. Phys. **B800**, 221 (2008).
[43] T. F. Feng, L. Sun, and X. Y. Yang, Phys. Rev. D **77**, 116008 (2008).
[44] G. Aad *et al.* (ATLAS Collaboration), Phys. Lett. B **796**, 68 (2019).
[45] G. Cacciapaglia, C. Csaki, G. Marandella, and A. Strumia, Phys. Rev. D **74**, 033011 (2006).
[46] M. Carena, A. Daleo, B. A. Dobrescu, and T. M. P. Tait, Phys. Rev. D **70**, 093009 (2004).
[47] F. Mamoudi, J. High Energy Phys. 12 (2007) 026.
[48] K. A. Olive and L. Velasco-Sevilla, J. High Energy Phys. 05 (2008) 052.
[49] B. O'Leary, W. Porod, and F. Staub, J. High Energy Phys. 05 (2012) 042.
[50] X. X. Dong, T. F. Feng, H. B. Zhang, S.-M. Zhao, and J.-L. Yang, J. High Energy Phys. 12 (2021) 052.
[51] R. L. Workman *et al.* (Particle Data Group), Prog. Theor. Exp. Phys. **2022**, 083C01 (2022).
[52] G. Aad *et al.* (ATLAS and CMS Collaborations), Phys. Rev. Lett. **114**, 191803 (2015).
[53] M. Aaboud *et al.* (ATLAS Collaboration), Phys. Lett. B **784**, 345 (2018).
[54] A. M. Sirunyan *et al.* (CMS Collaboration), Phys. Lett. B **805**, 135425 (2020).
[55] B. Abi *et al.* (Muon g-2 Collaboration), Phys. Rev. Lett. **126**, 141801 (2021).
[56] A. Dedes, M. Paraskevas, J. Rosiek, K. Suxho, and K. Tamvakis, J. High Energy Phys. 06 (2015) 151.
[57] J. Rosiek, Comput. Phys. Commun. **201**, 144 (2016).
[58] J. Hisano, T. Moroi, K. Tobe *et al.*, Phys. Lett. B **357**, 579 (1995).
[59] R. Barbieri, L. Hall, and A. Strumia, Nucl. Phys. **B445**, 219 (1995).
[60] J. Hisano, T. Moroi, K. Tobe, and M. Yamaguchi, Phys. Rev. D **53**, 2442 (1996).